Inorganic Chemistry

Article

pubs.acs.org/IC

First-Principles Screening of Complex Transition Metal Hydrides for High Temperature Applications

Kelly M. Nicholson and David S. Sholl*

School of Chemical & Biomolecular Engineering, Georgia Institute of Technology, 311 Ferst Drive, Atlanta, Georgia 30332-0100, United States

Supporting Information

ABSTRACT: Metal hydrides with enhanced thermodynamic stability with respect to the associated binary hydrides are useful for high temperature applications in which highly stable materials with low hydrogen overpressures are desired. Though several examples of complex transition metal hydrides (CTMHs) with such enhanced stability are known, little thermodynamic or phase stability information is available for this materials class. In this work, we use semiautomated thermodynamic and phase diagram calculations based on density functional theory (DFT) and grand canonical linear programming (GCLP) methods to screen 102 ternary and quaternary CTMHs and 26 ternary saline hydrides in a library of over 260 metals, intermetallics, binary, and higher hydrides to identify materials that release hydrogen at higher temperatures than the associated binary hydrides and at elevated temperatures, T > 1000 K, for 1 bar H_2 overpressure. For computational efficiency, we employ a tiered screening approach based first on solid phase ground state energies with temperature effects controlled via H_2 gas alone and second on the inclusion of phonon calculations that correct solid phase free energies for temperature-dependent vibrational contributions. We successfully identified 13 candidate CTMHs including Eu_2RuH_6, Yb_2RuH_6, Ca_2RuH_6, Ca_2OsH_6, Ba_2RuH_6, $Ba_3Ir_2H_{12}$, Li_4RhH_4, $NaPd_3H_2$, Cs_2PtH_4, K_2PtH_4, Cs_3PtH_5, Cs_3PdH_3, and Rb_2PtH_4. The most stable CTMHs tend to crystallize in the Sr_2RuH_6 cubic prototype structure and decompose to the pure elements and hydrogen rather than to intermetallic phases.

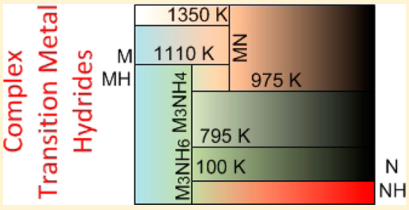

INTRODUCTION

Recent research efforts regarding hydrogen storage in solid metal hydrides have focused on applications for materials of moderate thermodynamic stability, that is, those that operate at or near ambient conditions, such as the onboard storage of hydrogen for use in fuel cell vehicles.[1−9] A convenient measure of thermodynamic stability is the temperature, T_d, at which a metal hydride is in thermal equilibrium with P = 1 bar H_2. If heated above this temperature, the metal hydride will release hydrogen gas. Relatively less attention has been paid to applications for metal hydrides of high stability, for example, T_d > 600 K, such as neutron moderators or nuclear fuel components in nuclear reactors[10−16] or as potential thermochemical media in solar energy storage systems.[17−20] If materials of suitable high thermodynamic stability can be identified, metal hydrides may also be deployed as tritium getterers in the U.S. Department of Energy proposed next generation nuclear plant (NGNP). The NGNP will use a very high temperature helium-cooled reactor with core outlet temperatures in the range of 1000 < T (K) < 1200.[21−25] The helium coolant may be used to provide high temperature process heat to industrial users if the radioactive tritium contaminant generated in the fission process can be removed. Because of the hazards and practical difficulties associated with performing experiments involving tritium at high temperature, computational methods based on density functional theory (DFT) provide an important tool for down-selecting interesting materials for this and other high temperature metal hydride applications since DFT provides reasonable accuracy in the prediction of thermodynamic properties for these systems.[26,27]

The thermodynamics of binary hydrides, M_xH_y (M = metal), are relatively well characterized in the literature, both experimentally and computationally.[26,28−33] Among the most stable binary hydrides are YH_2 (T_d > 1500 K[34]), ScH_2 (T_d > 1400 K[35]), and the series of rare earth hydrides.[36] Other metal hydrides with high thermodynamic stability have previously operated as neutron moderators, for example, ZrH_2 (LiH) with $T_d \approx$ 1154 K[37,38] (1184 K[39]), and titanium (T_d = 916 K for $TiH_{1.97}$[37,40]) and uranium (T_d = 705 K for UH_3[37,41]) hydrides are currently the preferred materials for long-term tritium storage.[42] Ternary and quaternary metal hydrides have representative stoichiometries $M_{1,x}$ $M_{2,y}$ H_z and $M_{1,w}$ $M_{2,x}$ $M_{3,y}$ H_z. These materials can be classified as interstitial hydrides in which hydrogen is taken up by the parent metal lattice, either an alloy or an intermetallic, without change in the crystal structure of the parent lattice or as complex hydrides, stabilized by charge transfer from a cationic species, typically an alkali, alkaline earth, or lanthanide element, to an anionic hydrido complex.[43,44] For most ternary hydrides of transition metals, the enthalpy of hydride formation, ΔH, is approximately a weighted sum of the heats of formation of the binary hydrides.[36,45,46] Assuming no kinetic limitations, a metastable

Received: August 15, 2014
Published: October 31, 2014

   dx.doi.org/10.1021/ic501990p | Inorg. Chem. 2014, 53, 11833−11848

ternary hydride will dissociate into a thermodynamically preferred mixture of the binary hydrides, binary alloys and/or intermetallics, and parent metals when heated. In these cases, the binary hydride defines the most thermodynamically stable hydride phase that forms in the element space. For the purposes of the NGNP and other high temperature metal hydride applications, this would indicate that binary hydrides with largely known thermodynamic properties form the upper (lower) boundary on the potential operating temperature (hydrogen equilibrium pressure) of metal hydrides.

There are a few materials for which it is known experimentally that the ternary hydride exhibits lower hydrogen equilibrium pressures at a given temperature than the strongest binary hydride that forms from the parent metals, that is, higher T_d. Recently, we used DFT to investigate the Th−Zr−H system, for which a ternary interstitial-type hydride was experimentally observed to exhibit lower hydrogen overpressures at high temperature than the strong parent binary hydrides, ThH_2 and ZrH_2.[27] Our DFT methods found that the ternary hydride $ThZr_2H_6$ was thermodynamically comparable to the strongest binary hydride ZrH_2 over the entire studied temperature range, 0−2000 K at 1 bar H_2, and our calculations reproduced the experimental phase behavior with reasonable fidelity. However, the increase in thermodynamic stability of the ternary hydride phase was not significantly greater than the binary hydride within the uncertainty of the DFT methods. In the case of the complex hydrides, there are examples of complex transition metal hydrides (CTMHs) with significant increases in thermodynamic stability, as measured by T_d, over the strongest binary hydride that forms in the element space. The most well-studied CTMH system is Mg_2FeH_6 for which measurements of structural, vibrational, electronic, and thermodynamic properties have been made using both experimental measurements and first-principles predictions.[17,47−50] Characteristic experimental T_d values for Mg_2FeH_6 (MgH_2) are $T_d \approx 650-693$[51] and 580 K (540 K)[49] (estimated from van't Hoff plots). Other examples of CTMHs with enhanced stability include Rb_2ZnH_4 ($T_d \approx 640$ K[4]), Rb_3ZnH_5 ($T_d \approx 630$ K[4]), Cs_2ZnH_4 ($T_d \approx 645$ K[4]), and Cs_3ZnH_5 ($T_d \approx 625$ K[4]), compared with RbH ($T_d \approx 440$,[4] 636 K[52]) and CsH ($T_d \approx 440$,[4] 662 K[53]).

Because of the relatively high temperatures required to release hydrogen from CTMHs (most have T_d values > 570 K)[43] and low gravimetric hydrogen capacities, CTMHs have largely been ignored for the purposes of fuel cell hydrogen storage, and little thermodynamic data is available. However, with their high stability, CTMH materials may be useful in high temperature applications such as the NGNP or concentrated solar plant chemical heat storage. As of 2005, there were 127 known CTMH materials that form from a wide range of cations and transition metal combinations.[43] The vast majority of these have little to no experimental data available beyond that of a crystal structure. These materials offer a rich landscape for exploring the thermodynamic stabilities of complex ternary hydrides with respect to the binary hydrides using DFT. In this Article, we use high throughput thermodynamic calculations based on DFT and phase diagram predictions based on grand canonical linear programming minimization (GCLP)[6,9,54−58] to characterize the thermodynamic stabilities of a large number of known CTMHs to identify materials with both enhanced stability relative to the associated binary hydrides ($T_d/T_{d,binary} \geq 1$) and high hydrogen release temperatures, taken here to be $T_d \geq 1000$ K. The final candidates will provide a useful upper boundary on the thermodynamic stabilities that can be reached based on known CTMH materials. Additionally, phase diagrams for final compounds communicate the relative thermodynamic stabilities of component compounds and relevant reaction schemes, which are valuable for determining processing conditions.[59]

CTMH Background. Yvon and Renaudin updated their comprehensive review of the known CTMHs in 2005.[43] To give an idea of the progress made in recent decades in reporting new CTMHs, consider that, in 1991, there were 13 CTMH structure types and in the latest 2005 update, there were 47 structure types or "prototypes" for over 127 unique compounds. CTMHs are stabilized via charge transfer from a cation, M, to an anionic transition metal hydrido complex, $[TrH_n]$. CTMHs form from late 3d, 4d, and 5d transition metals of groups 7−10 with monovalent alkali, divalent alkaline earth, and trivalent lanthanide species. Currently, no known transition metal hydrido complexes have been identified for elements of groups four, five, or six or of Ag, Au, or Hg.[43,60] There are two broad classifications of CTMHs that describe the types of hydrogen bonding in the material:[43] (1) Hydrogen covalently bound to a transition metal, Tr, to form anionic hydrido complexes, in which the charge on the complex is reduced and the structure is stabilized by surrounding cations:

$$M_m^{\delta+}[TrH_n]^{\delta-} \ (m, n, \delta = 1, 2, 3...) \quad (1)$$

(2) Composite hydrides that contain both hydrogen covalently bound to Tr to form complexes and anionic "intersitial" hydrogen that interact directly with the cations:

$$M_m^{\delta+}[TrH_n]^{\delta-}M_o^{\delta+}H_p^- \ (m, n, o, p, \delta = 1, 2, 3...) \quad (2)$$

$[TrH_n]$ tend to form for Tr in groups to the right of Mn, Tc, and Re (metals that do not form stable binary hydrides) on the periodic table. To the left of this group, interestitial binary hydrides are stable.[60] Two examples of CTMH crystal structures with the common six-coordinated octahedral and four-coordinated tetrahedral homonuclear $[TrH_n]$ complexes are shown in Figure 1. The most common arrangement of M is

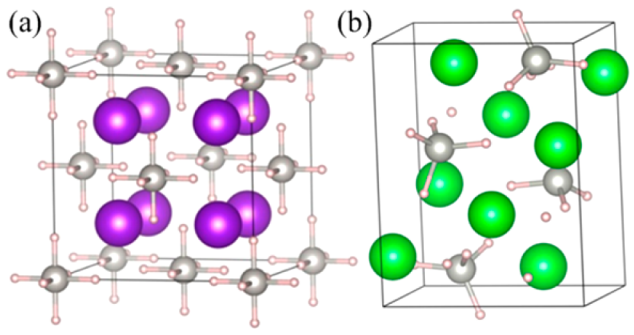

Figure 1. Representative crystal structures for (a) K_2PtH_6 (Sr_2PtH_6 prototype) with octahedral $[PtH_6]^{2-}$ complexes and (b) Sr_2PdH_4 (K_2ZnH_4 prototype) with tetrahedral $[PdH_4]^{4-}$ complexes. (largest sphere = K, Sr; medium sphere = Pt, Pd; smallest sphere = H).

the 8-fold cubic or nearly cubic structure. It has been argued that this arrangement allows cations to maximize interactions with hydrogen, stabilizing the overall structure.[43] For a given $[TrH_n]$ complex and different M species of the same valence, Tr−H bond lengths are relatively constant, and the M−H bond lengths scale with tabulated ionic radii.[43,50] Most CTMHs have closed outer electron shells and are diamagnetic. Some

dx.doi.org/10.1021/ic501990p | Inorg. Chem. 2014, 53, 11833−11848

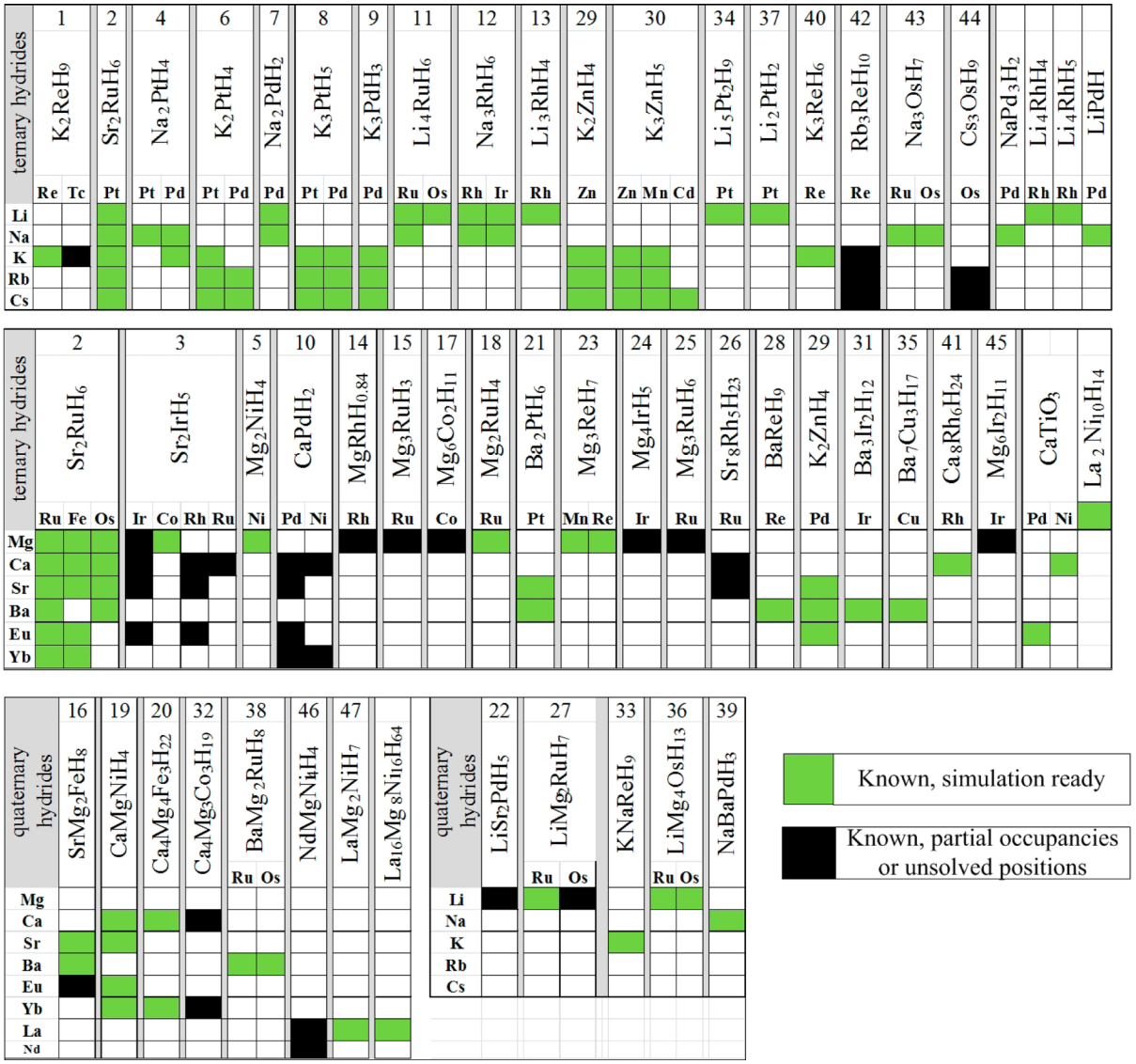

Figure 2. Experimentally known ternary (M−Tr−H) and quaternary (M_1−M_2−Tr−H) complex transition metal hydrides from the ICSD[61,62] and the Yvon and Renaudin 2005 review.[43] Numbers are consistent with Yvon and Renaudin[43] and describe the chronological discovery of the prototype ternary hydride M_x Tr_y H_z crystal structure shown vertically. Substitutional cations M of the same valence are grouped vertically. Substitutional transition metals Tr are listed horizontally. Simulation ready implies completely solved and ordered structure with no partial occupancies.

exceptions include materials with magnetic ions that order magnetically at low T (e.g., K_3MnH_5).[43]

Figure 2 maps the known CTMHs with experimentally reported crystal structures compiled from both the 2005 Yvon and Renaudin review[43] as well as a survey of the Inorganic Crystal Structure Database (ICSD)[61,62] for stoichiometric materials with CTMH-like compositions. The numeric classifications are consistent with the prototype numbering system of Yvon and Renaudin and describe the chronological order in which the prototype structure (chemical formula shown in figure) was reported. Prototypes without a numeric classifier were reported in the ICSD, but not in the review. Alkali, alkaline earth, and lanthanide M species are arranged vertically. Transition metal Tr species follow horizontally. Simulation ready implies that crystal structures are fully ordered, with no partial occupancies, and all atom positions resolved. Only simulation ready ICSD entries are shown in Figure 2. $EuPdH_3$ and $CaNiH_3$ are listed in the Yvon and Renaudin review as crystallizing with the $CaPdH_2$ prototype PM3M structure, characterized by disorder and partial hydrogen occupancies. However, given that the ICSD entries for these two materials list the prototype structure as $CaTiO_3$ and there are no partial occupancies for that stoichiometry, we additionally report these materials with the $CaTiO_3$ prototype in Figure 2. Also, LiPdH and Na_3PdH_2 structures are shown as CTMHs in Figure 2 because of their structural similarities with the other materials. However, as Yvon and Renaudin note in the review, these materials have only a weak tendency toward complex formation.[43]

Despite their potential high hydrogen volumetric storage capacities, the high thermal stabilities of CTMHs have currently made them unattractive for ambient condition fuel cell applications. Computational and experimental studies into the thermodynamics or kinetics of hydride systems have focused, instead, on the light complex hydrides, such as the borohydrides and alanates.[6−9,33,54−58,63−74] Primarily, DFT calculations have been used to predict the bulk structural properties and vibrational densities of states (VDOS) of

dx.doi.org/10.1021/ic501990p | Inorg. Chem. 2014, 53, 11833−11848

CTMHs.[60,75−78] To date, there has been no large scale computational screening of CTMHs for high temperature hydrogen storage applications. This work is the first to systematically study the relative thermodynamic stabilities of all simulation ready CTMHs using DFT.

As previously discussed, charge transfer from M to $[TrH_n]$ stabilizes CTMHs. Several studies have shown that the electronegativity of the cation is a good predictor of the standard heat of formation of complex hydrides.[50,63−65] However, this approach does not take into account the relative stabilities of competing compounds such as intermetallics or binary hydrides that could form in an element space. Our approach avoids this uncertainty since phase diagrams are generated for given element combinations, computing the thermodynamically preferred mix of compounds from a library of potential compounds at a given hydrogen chemical potential.

Screening Algorithm. We aim to identify known or "existing" CTMH candidate materials that are both more stable than the binary hydrides that form from the constituent metals and that release hydrogen only at high temperature. For computational efficiency, we use two rounds of screening at increasing levels of theory, down-selecting interesting element spaces and, therefore, the CTMH candidates, with each step.

In round 1, we compute phase diagrams at P = 1 bar H_2 and $0 \leq T$ (K) ≤ 2000 (using methods described in detail below), while ignoring the vibrational Helmholtz free energies of the solid phases for the 72 element spaces (57 M−Tr−H ternary and 15 M_1−M_2−Tr−H quaternary) shown in Figure 3 using a simulation ready DFT materials library (260+ materials) summarized in Table 1. This initial materials library is available in its entirety in Table S.1 in the Supporting Information. We exclude materials that are not simulation ready such as those with partial occupancies, for example, materials that crystallize in the 10−Ca_2PdH_2 prototype with 2/3 occupancy of all H sites or 15−Mg_3RuH_3 with 1/2 occupancy of the 8i H sites, etc. Similarly, only intermetallics with fully ordered structures are included in our library. In Figure 3, cations are arranged according to valence and transition metals according to group number and molecular weight for the ternary hydrides. Each targeted element space contains at least one CTMH candidate material from Figure 2. Ternary alkaline earth (saline) hydrides (e.g., $Ba_2Mg_3H_{10}$ and $Mg_3Sr_2H_{10}$) are not strictly CTMHs but form in the element spaces under consideration and are screened as a result. We include 95 fully ordered binary intermetallics. It is notable that just over half of the element spaces with a CTMH under consideration do not contain binary intermetallics that are experimentally known. This reflects the fact that most CTMHs are true ternary compounds that do not derive from the hydrogenation of stable intermetallics.[43] Ten of the element spaces account for 54 of the 95 intermetallics, which indicates that the presence of intermetallics is highly concentrated among certain element combinations.

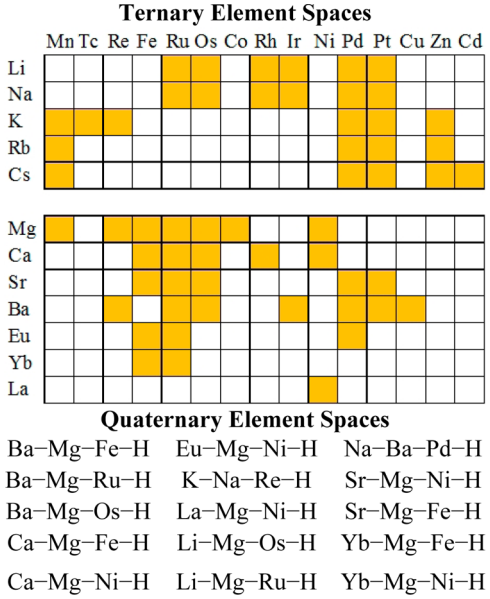

Figure 3. Ternary M−Tr−H (orange) and quaternary M_1−M_2−Tr−H element spaces (element combinations) studied with the round 1 level of screening, based on simulation ready CTMHs from Figure 2. Transition metals, Tr, for ternary spaces are listed horizontally. Alkali and alkaline earth metals are listed vertically. Element combinations not listed or shaded were not included in the overall screening.

Table 1. Summary of Initial DFT Materials Library for Screening of Existing CTMHs Listed in Table S.1 in the Supporting Information

material type	number of compounds
ternary CTMHs	84
quaternary CTMHs	18
binary hydrides	23
ternary alkaline earth (saline) hydrides	18
pure metals	28
binary intermetallics	95

In the first round of screening, finite temperature contributions for the condensed phases are ignored. We retrieve an estimate of the relative and absolute stabilities of hydride phases that form in each element space, and retain those element spaces that contain a CTMH with enhanced stability with respect to the binary hydrides, $T_d/T_{d,binary} \geq 1$. At this step we do not require that all hydrides operate at high temperature $T_d \geq 1000$ K since T_d can change in either direction when including vibrational contributions. This might also affect the stability of the higher hydride with respect to the binary hydride, but we feel applying this screening criterion is reasonably conservative while allowing us to down select to a manageable number of materials to study at the higher level of theory.

In round 2 of our screening, we perform calculations, hereafter referred to as phonon calculations, to include vibrational contributions within the harmonic level of theory for the materials in element spaces retained from round 1. We recompute phase diagrams while taking into account finite temperature vibrational effects of the solid phases. This provides our best estimate of the relative stabilities of CTMH candidates with respect to the binary hydrides and other materials. Additionally, compounds that are dynamically stabilized through vibrational contributions may be revealed in the set of stable compounds as a function of hydrogen chemical potential. Final candidates are chosen to be those with enhanced stability relative to the binary hydrides, $T_d/T_{d,binary} \geq 1$, and $T_d \geq 1000$ K.

In this study, we consider only those compounds that have been observed experimentally with either a simulation ready crystal structure available in the ICSD or a template material with the same prototype crystal structure with all atomic

dx.doi.org/10.1021/ic501990p | Inorg. Chem. 2014, 53, 11833−11848

positions resolved. Our calculations cannot make predictions about the stabilities of compounds not included in the DFT materials library. It is possible that either a stable ternary or higher hydride phase exists with higher T_d than our final candidates, but has not yet been experimentally observed, or that a high temperature intermetallic or alloy phase exists that is not included in our library that may destabilize our final candidates. Our calculations, however, are useful for rapidly characterizing thermodynamic properties, such as heats of dehydrogenation and for identifying decomposition pathways for a large set of interesting materials at a moderate level of theory. Then, more rigorous thermodynamic data regarding ΔH, ΔS, and equilibrium pressures as a function of temperature can be obtained that can be directly related to experimental measurements. Recently, we have used calculations to calibrate the accuracy of DFT in determining the thermodynamics of five binary hydrides, including NaH, LiH, TiH_2, ZrH_2,and HfH_2, that release hydrogen at decomposition temperatures, T_d, in the range 400−1200 K for P = 1 bar hydrogen.[26] We found that predictions of T_d within the simple harmonic level of theory using the projector-augmented wave (PAW) method with the generalized gradient approximation (GGA) and PW91 exchange-correlation functional were accurate to within 130 K for the alkali hydrides and to within 50 K for the transition metal hydrides, which is sufficient for screening purposes. This is in line with previous DFT calculations that estimated that the uncertainty in the DFT-predicted reaction enthalpies $\Delta H(T)$ for light metal hydride hydrogen release reactions (predicted at the harmonic level of theory using the same DFT functionals) to be within ±10 kJ mol^{-1} H_2 of the experimental value.[6,7] On a T_d basis, this uncertainty corresponds to approximately 75−105 K, based on $T_d = \Delta H(T)/\Delta S(T)$ and assuming a constant ΔS = 0.130 kJ K^{-1} mol^{-1} H_2 for reaction entropies dominated by the H_2 gas contribution,[3] and ΔS = 0.097 kJ K^{-1} mol^{-1} H_2 for light metal complex reactions, such for $LiBH_4 \rightarrow LiH + B + 3/2H_2$.[7]

THEORY

Our method for predicting the thermodynamically stable mixture for a given set of compounds that could potentially form in an element space is similar to that described in our previous work for the Th−Zr−H system.[27] Given that we apply the GCLP method to quaternary, as well as ternary element spaces, we develop the equations here to apply to a general element space. We have used the pymatgen[79] software to perform the grand potential minimization and phase diagram predictions, and so we build upon the nomenclature of Ong, Ceder and colleagues for consistency.[59,80]

For an isobaric, isothermal system that is open to a hydrogen atmosphere, the thermodynamic phase equilibria can be described by the hydrogen grand potential

$$\varphi(T, P, N_j, \mu_{H_2}) = G(T, P, N_j, \mu_{H_2}) - \mu_{H_2} N_{H_2}(T, P, N_j, \mu_{H_2}) \quad (3)$$

where N_j refers to the number of atoms of non-H species j. Here, we limit our study to ternary N_1−N_2−H and quaternary N_1−N_2−N_3−H spaces. Primarily, we are interested in probing the relative stabilities of condensed phases for which $(P\Delta V)_{solids} \ll P_{H_2}$, and so we ignore the PV contributions for solid components. In this work, only ordered compounds without partial occupancies are considered, and the free energy for solid compounds is described by

$$G_j(T) \approx F_j(T) = E_{0,j} + F_j^{vib}(T) \quad (4)$$

without configurational or electronic entropy contributions. We normalize eq 3 with respect to the non-H species to give

$$\bar{\varphi}(T, P, x_j, \mu_{H_2}) \approx \frac{E_0 + F^{vib}(T) - \mu_{H_2} N_{H_2}}{\sum_j^n N_j} \quad (5)$$

where the fractional component of j in the mixture is

$$x_j = \frac{N_j}{\sum_j N_j} \quad (6)$$

and $\sum_j x_j = 1$.

In these open metal−hydrogen systems, a simplifying assumption can be made that changes in the stable mixture of compounds are mainly because of the uptake or release of hydrogen gas such that the reaction entropy is dominated by the hydrogen gas entropy. Additionally, it is assumed that the zero point vibrational energy contribution of the solid phases is negligible compared with the change in ground state electronic energy. Under these approximations, temperature effects are controlled through the hydrogen chemical potential and eq 5 reduces to

$$\bar{\varphi}(T, P, x_j, \mu_{H_2}) \approx \frac{E_0 - \mu_{H_2} N_{H_2}}{\sum_j^n N_j} \quad (7)$$

Equation 7 is useful because it allows us to compute an approximate phase diagram using only DFT energies for a set of solid compounds (round 1). Interesting systems can then be studied with the more rigorous eq 5 using phonon calculations to determine $F^{vib}(T)$ for each solid (round 2).

The hydrogen chemical potential is defined as

$$\mu_{H_2}(T, P_{H_2}) = \mu_{H_2}(T, P_0) + k_B T \ln \frac{P_{H_2}}{P_0} \quad (8)$$

which relates the temperature and partial pressure of hydrogen.[59] Here, $\mu_{H_2}(T,P_0)$ is the chemical potential at a reference pressure P_0 = 1 bar. The chemical potential of hydrogen at P_0 is taken to be the Gibbs free energy of the ideal diatomic gas

$$\mu_{H_2}(T, P_0) \approx G_{H_2}(T, P_0) = H_{H_2}(T, P_0) - TS_{H_2}(T, P_0) \quad (9)$$

where[7]

$$G_{H_2} = U_{0,H_2} + U_{trans+rot,H_2}(T) + U_{vib,H_2}(T) - TS_{H_2}(T) + (PV)_{H_2} \quad (10)$$

Here, G is calculated using a combination of DFT-computed, statistical mechanical, and tabulated results. U_{0,H_2} was computed using DFT as the total electronic energy of a hydrogen molecule in a 10 Å simulation box. The translational, rotational, and vibrational terms were determined via[81,82]

$$U_{trans+rot,H_2} = \frac{5}{2}RT \quad (11)$$

and

dx.doi.org/10.1021/ic501990p | Inorg. Chem. 2014, 53, 11833−11848

$$U_{\mathrm{vib,H_2}}(T) = \frac{N_A h\nu}{2} + \frac{N_A h\nu e^{-\beta h\nu}}{1 - e^{-\beta h\nu}} \quad (12)$$

where N_A is Avogadro's number, h is Planck's constant, $\beta = (k_B T)^{-1}$, and ν is the H_2 vibrational frequency.[39,40] We determined ν within the harmonic approximation using DFT to be 1.310×10^{14} s^{-1}, which corresponds to a zero point energy of ~26.1 kJ mol^{-1}, very close to the experimental value of 25.1 kJ mol^{-1} and the value obtained by Alapati et al. with similar DFT calculations.[7,83] Since we assume hydrogen behaves as an ideal gas, $(PV)_{H_2} = RT$. We compute S_{H_2} using

$$S\ (\mathrm{J\ mol^{-1}\ K^{-1}}) = 29.562647 \ln T - 37.482701 \quad (13)$$

which reflects a fitting of NIST-JANAF tabulated values for the entropy of diatomic hydrogen gas for $100 \leq T\ (\mathrm{K}) \leq 2000$ at 1 bar.[84] This fitting results in an error of less than 1 kJ mol^{-1} H_2 for TS contributions to the free energy for temperatures up to 2000 K. This approach to computing the chemical potential of hydrogen differs from that of Alapati et al.[6] who determined the temperature-dependent portion of the chemical potential using the partition function directly. However, our method results in less than a 0.5 kJ mol^{-1} difference in the chemical potential at P = 1 bar for the studied temperature range, and it allows us to clearly separate enthalpic and entropic effects for computing thermodynamic properties.

COMPUTATIONAL METHODS

Plane-wave DFT calculations were carried out via VASP[85−89] using the projector augmented wave method (PAW) with the PW91 GGA exchange-correlation functional.[90−92] Pseudopotentials for each element were taken to be the recommended PAW potentials listed in the VASP manual.[93] Experimental crystal structures for the low temperature, low pressure forms of target compositions were taken from the ICSD.[61,62] We utilized pymatgen automation tools to manage the DFT computation setup and Custodian for error handling.[79,94] These software allow us to efficiently perform calculations for the large set of materials considered in this work and to streamline the workflow.

Volume, shape, and ion position relaxations were performed on primitive cells for each compound using the conjugate gradient method until forces on each atom were less than 0.03 eV $Å^{-1}$ and electronic steps were converged to within 10^{-5} eV. We used Methfessel−Paxton smearing with width of 0.2. Based on initial convergence testing for a number of materials, described in the Supporting Information (Figures S.1 and S.2), we applied a cutoff energy of 400 eV and a minimum density of 4000 k-points/(number of atoms per unit cell) distributed as evenly as possible along the reciprocal lattice vectors. Monkhorst−Pack meshes were used for all symmetries except hexagonal, for which we adopted Γ-centered grids for faster convergence.

For each material, we performed spin-polarized DFT calculations for one step on the initial crystal structure, adopting high spin states for magnetic elements ferromagnetically.[94] In the style of Curtarolo et al., if after one step the magnetic moment was less than 0.025 μ_B $atom^{-1}$, indicating that the influence of spin is negligible on the ground state energy, we turned spin off and relaxed the geometries as described above.[95] However, if the magnetic moment was greater than 0.025 μ_B $atom^{-1}$, we continued volume relaxations with spin-polarization activated. For computational speed, we made no attempt to search for antiferromagnetic ground states, particularly since most known CTMHs are diamagnetic. However, interesting materials could be studied more rigorously if the magnetic properties were desired.

Phonon calculations were performed for materials in element spaces retained for round 2 screening. Initial convergence testing of the vibrational free energy with respect to supercell size was carried out for a number of materials, described in the Supporting Information (Figure S.3). Except where indicated, 2 × 2 × 2 supercells were adopted and k-points adjusted to maintain the same grid density. Hexagonal structures were studied in the rhombohedral settings following the guidelines of Parlinski.[96] We first relaxed volume, shape, and ion positions using the conjugate gradient method until forces on each atom were less than 10^{-4} eV $Å^{-1}$ and electronic steps were converged to within 10^{-7} eV. To determine $F^{vib}(T)$, we computed the VDOS for each compound within the harmonic approximation based on the supercell approach using a default atomic displacement of ±0.01 Å.[97] Uniform q-point sampling meshes were used to sample the Fourier components of the dynamical matrix such that F^{vib} at 2000 K for each compound was converged to within 1 kJ mol^{-1}.

RESULTS AND DISCUSSION

Round 1. Crystal structures for >260 materials were relaxed with moderate force and electronic energy convergence thresholds to obtain ground state DFT energies. The DFT-relaxed structural parameters as well as the experimental values for these materials are available in Table S.1 in the Supporting Information. Figures 4 and 5 present a comparison of the

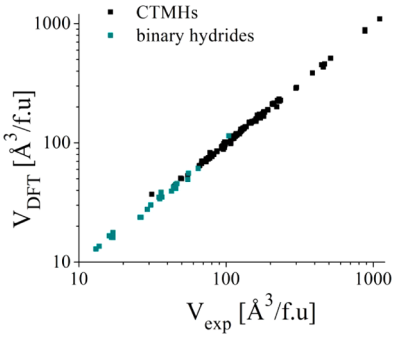

Figure 4. Comparison of the experimental and relaxed DFT volumes for the known complex transition metal hydrides, saline hydrides, and binary hydrides studied at the round 1 level of screening.

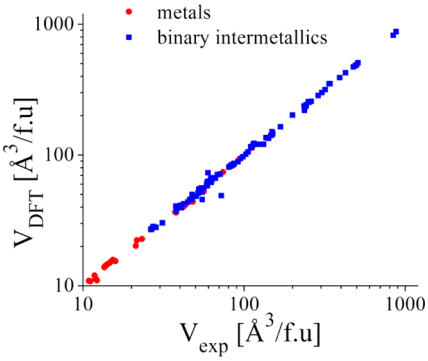

Figure 5. Comparison of the experimental and relaxed DFT volumes for the metals and binary intermetallics studied at the round 1 level of screening.

predicted and experimental unit cell volumes. As expected, the overall agreement is good. For the metals, binary intermetallics, and ternary hydrides, more than 85% of DFT-predicted volumes are within 5% of the experimental value. The agreement is slightly less accurate for the binary hydrides with 85% of the 23 DFT-predicted volumes within 9% of the experimental value. However, previous calculations have shown that DFT using Perdew−Wang GGA functionals like those utilized here tend to predict the enthalpies of formation for binary hydrides to within a typical accuracy of 10−20 kJ mol^{-1}

dx.doi.org/10.1021/ic501990p | Inorg. Chem. 2014, 53, 11833−11848

H_2, which we expect to be sufficient for our screening purposes.[9,98]

There are several compounds for which our DFT-predicted volumes and the experimental volumes differ by more than ∼10%. For these, we compare our predicted structures with structures calculated by the Materials Project (MP),[79,99] an online database of over 80 000 materials with properties based on high-throughput DFT calculations. The DFT calculation details of this work and the current MP are not identical and not all of the compounds considered in this screening are included in the MP database. However, the MP provides a good check for consistency at least within DFT GGA methods. The materials for which predicted and experimental volumes vary by more than ∼10% are listed in Table 2.

Table 2. Comparison of Unit Cell Volumetric Errors (with Respect to the Experimental Value) Obtained Using DFT with Round 1 [Round 2] Convergence Criteria for This Work and the Materials Project DFT-Based Materials Database[79,99]

material	this work (%)	Materials Project (%)
Mn	−9.8	7.4
Yb_3H_8	9.5 [8.8]	13.1
Ni_2H	−10.4 [−11.6]	−11
RbH	−10.2 [<2]	0.01
SrH_2	−8.8 [∼3]	−1.5
MgSr	22.7	23.4
Cs_3MnH_5	−9.3	1.8
$EuFe_2$	−32.3	no entry
$EuNi_2$	−17.0	no entry
LiPdH	18.4	no entry

Continued relaxation of the unit cells for RbH and SrH_2 to the higher convergence criteria required for round 2 phonon calculations brings the predicted DFT volumes into line with those predicted by the MP and experiment. However, continued relaxations do not improve agreement for Yb_3H_8 or Ni_2H, but errors relative to the experimental volumes are roughly the same for this work as in the MP. These binary hydrides are not critical to the screening of high temperature CTMHs since both materials decompose at low temperatures. While our calculations do obtain agreement with the MP for the ground state magnetic moments of pure Fe, Co, and Ni, the DFT methods used here do not rigorously search for the optimal spin state of magnetic materials in general, which could account for the disagreement in the case of $EuFe_2$ and $EuNi_2$. Our calculations fail to predict the same magnetic ground state for Mn and Cs_3MnH_5 as predicted with the MP, which likely accounts for underestimation of the predicted volumes. Therefore, heats of formation for reactions with Mn-based compounds may have larger errors than otherwise expected. If potentially interesting ternary hydrides of Eu−Fe, Eu−Ni, or Cs−Mn are identified, more detailed DFT methods could be used to obtain global magnetic ground state of these materials to improve estimates of the CTMH relative stabilities.[94] Reasons for the discrepancy in the DFT-predicted and experimental LiPdH are not immediately apparent. As an additional check, we relaxed the experimental structure allowing only the atom positions to move while maintaining the unit cell volume and also relaxed the DFT-predicted structure allowing all degrees of freedom to change such that forces on each atom were less than 10^{-4} eV Å and the electronic energy steps were converged to 10^{-7} eV, two high accuracy conditions. The DFT-predicted structure is 0.84 eV lower in energy than the experimental structure indicating that the DFT structure is a more likely stable state.

We predicted phase diagrams at P = 1 bar H_2 for $0 \leq T$ (K) ≤ 2000 for the 72 element spaces in Figure 3 using eq 7, ignoring vibrational contributions to the free energies of solid phases. In lieu of presenting each individual diagram, Table 3 lists the decomposition (dehydrogenation) reactions for each metal hydride that is predicted to form within the conditions studied, the temperature of hydrogen release, and the enthalpy of reaction approximated by ΔE_0, again ignoring zero point vibrational energies. For comparison, available experimental data for the binary hydrides is presented in Table 4. We see that the DFT, even based on ground state energies alone, separates the binary hydrides into high and low temperature materials, although the relative stabilities of some materials are not reproduced exactly. In a similar fashion, it is expected that the DFT calculations can separate the ternary and higher CTMHs with reasonable fidelity.

In Table 3, 10 of the top 11 most thermodynamically stable CTMHs crystallize in the 2−Sr_2RuH_6 cubic crystal structure with metal cations that form very strong binary hydrides. Additionally, of the top 11 most thermodynamically stable CTMHs, only the Yb−Ru−H and Eu−Fe−H systems have a single binary intermetallic in the accompanying phase spaces. The presence of stable intermetallic phases tends to destabilize ternary hydrides.

Figure 6 shows the absolute and relative decomposition temperature screening criteria for each studied CTMH. Figure S.4 in the Supporting Information shows a similar plot for the saline hydrides. Along the vertical axis, decomposition temperatures are normalized by the most stable binary hydride that forms in a given element space, and materials normalized by the same binary hydride therefore form lines. Of the 102 CTMHs, 40 ternary hydrides have $T_d/T_{d,binary} \geq 1$, with 15 of these releasing H_2 at temperatures greater than 1000 K. No quaternary or ternary alkaline earth (saline) hydrides were predicted to have this enhanced stability relative to the binary hydrides. The most stable quaternary hydride of those studied is $SrMgNiH_4$, which decomposes to a mixture of the binary hydride SrH_2 and Mg−Ni intermetallics. Overall, we retain 31 of the original 72 element spaces for round 2 screening, summarized in Figure 7. Although Mg_3MnH_7 is predicted to have a modest enhanced stability factor of ∼1.17, we do not study this element space at the higher level of theory due to the computational expense of searching for appropriate ground state spin states.

Table 5 lists the experimentally observed compounds that were not predicted to be thermodynamically stable based on round 1 GCLP minimizations along with the energy above the convex hull for each phase. A positive convex hull energy describes the decomposition energy of a given phase into the thermodynamically preferred mixture of adjacent phases.[68] A small value indicates that the phase is in close competition with another set of stable materials. Materials that appear in Table 5 may be dynamically stabilized through vibrational or kinetic effects. In general, pressure effects are small for condensed phases, but our calculations do not capture materials that are only thermodynamically stable at high pressures. However, the largest source of uncertainty in the calculation of energies results from the inability of the GGA pseudopotential to exactly describe exchange-correlation effects, which is an unavoidable

dx.doi.org/10.1021/ic501990p | Inorg. Chem. 2014, 53, 11833−11848

Table 3. Round 1 Metal Hydride Decomposition Reactions, Hydrogen Release Temperatures for 1 Bar H_2, T_d (K), and Ground State Reaction Energies (kJ mol^{-1} H_2)

metal hydride	T_d	decomposition reaction	ΔE_0
		binary hydrides	
SrH_2	1545	$SrH_2 \leftrightarrow Sr + H_2$	203.3
EuH_2	1485	$EuH_2 \leftrightarrow Eu + H_2$	193.2
YbH_2	1440	$YbH_2 \leftrightarrow Yb + H_2$	169.1
CaH_2	1380	$CaH_2 \leftrightarrow Ca + H_2$	175.1
LiH	1350	$2\,LiH \leftrightarrow 2Li + H_2$	168.7
LaH_3	1260	$^2/_3LaH_3 \leftrightarrow {}^2/_3La + H_2$	154.2
BaH_2	1140	$BaH_2 \leftrightarrow Ba + H_2$	150.6
KH	855	$2KH \leftrightarrow 2K + H_2$	86.6
NaH	855	$2NaH \leftrightarrow 2Na + H_2$	85.5
MgH_2	720	$MgH_2 \leftrightarrow Mg + H_2$	64.5
RbH	600	$2RbH \leftrightarrow 2Rb + H_2$	45.8
CsH	585	$2CsH \leftrightarrow 2Cs + H_2$	43.0
PdH	465	$2PdH \leftrightarrow 2Pd + H_2$	25.2
NiH	420	$2NiH \leftrightarrow 2Ni + H_2$	19.6
RhH	120	$2RhH \leftrightarrow 2Rh + H_2$	−18.4
		complex transition metal hydrides	
Eu_2RuH_6	1530	$^1/_3Eu_2RuH_6 \leftrightarrow {}^2/_3Eu + 1/3Ru + H_2$	200.7
Yb_2RuH_6	1500	$^1/_3Yb_2RuH_6 \leftrightarrow {}^1/_3Ru + {}^2/_3Yb + H_2$	196.8
Ca_2OsH_6	1425	$^1/_3Ca_2OsH_6 \leftrightarrow {}^2/_3Ca + {}^1/_3Os + H_2$	183.8
Ca_2RuH_6	1425	$^1/_3Ca_2RuH_6 \leftrightarrow {}^2/_3Ca + {}^1/_3Ru + H_2$	183.5
Sr_2RuH_6	1350	$Sr_2RuH_6 \leftrightarrow Ru + 2SrH_2 + H_2$	170.1
Sr_2OsH_6	1335	$Sr_2OsH_6 \leftrightarrow Os + 2SrH_2 + H_2$	165.8
Ba_2RuH_6	1305	$^1/_3Ba_2RuH_6 \leftrightarrow {}^2/_3Ba + {}^1/_3Ru + H_2$	161.2
Eu_2FeH_6	1305	$Eu_2FeH_6 \leftrightarrow 2EuH_2 + Fe + H_2$	161.5
Ba_2OsH_6	1275	$^1/_3Ba_2OsH_6 \leftrightarrow {}^1/_3Os + {}^2/_3Ba + H_2$	155.6
$Ba_3Ir_2H_{12}$	1275	$^1/_6Ba_3Ir_2H_{12} \leftrightarrow {}^1/_3Ir + {}^1/_2\,Ba + H_2$	157.1
Sr_2FeH_6	1245	$Sr_2FeH_6 \leftrightarrow Fe + 2SrH_2 + H_2$	151.2
K_2PtH_4	1215	$^1/_2K_2PtH_4 \leftrightarrow {}^1/_2Pt + K + H_2$	145.9
$Ca_8Rh_6H_{24}$	1200	$^1/_7Ca_8Rh_6H_{24} \leftrightarrow {}^3/_7CaRh_2 + {}^5/_7CaH_2 + H_2$	143.3
Na_2PdH_2	1185	$Na_2PdH_2 \leftrightarrow Pd + 2Na + H_2$	140.6
Rb_2PtH_4	1185	$^1/_2Rb_2PtH_4 \leftrightarrow {}^1/_2Pt + Rb + H_2$	141.0
Cs_2PtH_4	1170	$^1/_2Cs_2PtH_4 \leftrightarrow {}^1/_2Cs_2Pt + H_2$	138.8
Li_3RhH_4	1110	$Li_3RhH_4 \leftrightarrow 2LiH + LiRh + H_2$	127.5
Na_3IrH_6	1110	$^1/_3Na_3IrH_6 \leftrightarrow Na + {}^1/_3Ir + H_2$	128.5
Li_3IrH_6	1065	$^1/_2Li_3IrH_6 \leftrightarrow {}^1/_2IrLi + LiH + H_2$	121.2
Li_4OsH_6	1065	$Li_4OsH_6 \leftrightarrow 4LiH + Os + H_2$	119.9
$CaNiH_3$	1050	$^6/_5CaNiH_3 \leftrightarrow {}^4/_5CaH_2 + {}^2/_5CaNi_3 + H_2$	117.4
K_3PdH_3	1035	$^2/_3K_3PdH_3 \leftrightarrow {}^2/_3Pd + 2K + H_2$	114.8
Na_3RhH_6	1020	$^1/_3Na_3RhH_6 \leftrightarrow {}^1/_3Rh + Na + H_2$	112.5
$SrMgNiH_4$	1020	$SrMgNiH_4 \leftrightarrow SrH_2 + {}^1/_3Mg_2Ni + {}^1/_3MgNi_2 + H_2$	112.4
$BaMg_2OsH_8$	1005	$^2/_5BaMg_2OsH_8 \leftrightarrow {}^4/_5Mg + {}^1/_5Ba_2OsH_6 + {}^1/_5Os + H_2$	111.2
Cs_3PdH_3	1005	$^2/_3Cs_3PdH_3 \leftrightarrow {}^2/_3Pd + 2Cs + H_2$	109.6
Sr_2PdH_4	1005	$Sr_2PdH_4 \leftrightarrow SrH_2 + PdSr + H_2$	111.3
$Yb_4Mg_4Fe_3H_{22}$	1005	$^1/_7Yb_4Mg_4Fe_3H_{22} \leftrightarrow {}^4/_7Mg + {}^3/_7Fe + {}^4/_7YbH_2 + H_2$	111.5
Ba_2PdH_4	975	$Ba_2PdH_4 \leftrightarrow BaPd + BaH_2 + H_2$	106.1
$BaMg_2FeH_8$	975	$^{17}/_{55}BaMg_2FeH_8 \leftrightarrow {}^{17}/_{55}Fe + {}^2/_{55}Ba_2Mg_{17} + {}^{13}/_{55}BaH_2 + H_2$	104.9
$Ca_4Mg_4Fe_3H_{22}$	975	$1/7Ca_4Mg_4Fe_3H_{22} \leftrightarrow 3/7Fe + 4/7Mg + 4/7CaH_2 + H_2$	105.1
$EuMgNiH_4$	960	$EuMgNiH_4 \leftrightarrow {}^1/_3Mg_2Ni + {}^1/_3MgNi_2 + EuH_2 + H_2$	103.8
Mg_2OsH_6	960	$^1/_3Mg_2OsH_6 \leftrightarrow {}^1/_3Os + {}^2/_3Mg + H_2$	103.9
Na_2PtH_4	960	$^1/_2Na_2PtH_4 \leftrightarrow 0.25NaPt_2 + 0.75Na + H_2$	102.8
Rb_3PdH_3	960	$^2/_3Rb_3PdH_3 \leftrightarrow 2Rb + {}^2/_3Pd + H_2$	102.8
$BaMg_2RuH_8$	945	$^2/_5BaMg_2RuH_8 \leftrightarrow {}^1/_{10}Mg_3Ru_2 + {}^1/_2Mg + {}^1/_5Ba_2RuH_6 + H_2$	100.5
Mg_2RuH_4	945	$^1/_2Mg_2RuH_4 \leftrightarrow {}^1/_4Mg_3Ru_2 + {}^1/_4Mg + H_2$	101.2
Na_4RuH_6	945	$^1/_3Na_4RuH_6 \leftrightarrow {}^1/_3Ru + {}^4/_3Na + H_2$	101.9
Cs_2PdH_4	930	$Cs_2PdH_4 \leftrightarrow {}^2/_3Cs_3PdH_3 + {}^1/_3Pd + H_2$	97.5
K_2PdH_4	930	$K_2PdH_4 \leftrightarrow {}^2/_3K_3PdH_3 + {}^1/_3Pd + H_2$	97.6
$LiMg_2OsH_7$	930	$2LiMg_2OsH_7 \leftrightarrow {}^3/_2Mg_2OsH_6 + Mg + {}^1/_2Li_4OsH_6 + H_2$	97.9

dx.doi.org/10.1021/ic501990p | Inorg. Chem. 2014, 53, 11833−11848

Table 3. continued

metal hydride	T_d	decomposition reaction	ΔE_0
		complex transition metal hydrides	
$LiMg_4Os_2H_{13}$	930	$2LiMg_4Os_2H_{13} \leftrightarrow {}^{7}/_{2}Mg_2OsH_6 + Mg + {}^{1}/_{2}Li_4OsH_6 + H_2$	98.5
Rb_2PdH_4	930	$Rb_2PdH_4 \leftrightarrow {}^{2}/_{3}Rb_3PdH_3 + {}^{1}/_{3}Pd + H_2$	99.3
Sr_2PtH_6	930	$^{4}/_{9}Sr_2PtH_6 \leftrightarrow {}^{1}/_{9}Pt_4Sr_5 + {}^{1}/_{3}SrH_2 + H_2$	98.2
$SrMg_2FeH_8$	930	$^{2}/_{5}SrMg_2FeH_8 \leftrightarrow {}^{1}/_{5}Sr_2FeH_6 + {}^{1}/_{5}Fe + {}^{4}/_{5}Mg + H_2$	98.4
Ba_2PtH_6	900	$^{1}/_{2}Ba_2PtH_6 \leftrightarrow {}^{1}/_{2}BaPt + {}^{1}/_{2}BaH_2 + H_2$	94.4
Mg_2FeH_6	900	$^{1}/_{3}Mg_2FeH_6 \leftrightarrow {}^{2}/_{3}Mg + {}^{1}/_{3}Fe + H_2$	92.9
Cs_2ZnH_4	885	$^{1}/_{2}Cs_2ZnH_4 \leftrightarrow {}^{1}/_{2}Zn + Cs + H_2$	90.7
Li_2PdH_2	885	$2Li_2PdH_2 \leftrightarrow 2LiH + 2LiPd + H_2$	98.1
Na_3OsH_7	885	$^{2}/_{7}Na_3OsH_7 \leftrightarrow {}^{6}/_{7}Na + {}^{2}/_{7}Os + H_2$	90.8
Yb_2FeH_6	885	$Yb_2FeH_6 \leftrightarrow Fe + 2YbH_2 + H_2$	90.1
$NaBaPdH_3$	870	$^{6}/_{5}NaBaPdH_3 \leftrightarrow {}^{6}/_{5}Na + {}^{2}/_{5}Ba_2PdH_4 + {}^{2}/_{5}BaPd_2 + H_2$	89.5
$EuPdH_3$	855	$EuPdH_3 \leftrightarrow {}^{1}/_{2}EuPd_2 + {}^{1}/_{2}EuH_2 + H_2$	84.9
Mg_2CoH_5	855	$^{2}/_{5}Mg_2CoH_5 \leftrightarrow {}^{1}/_{5}Co_2Mg + {}^{3}/_{5}Mg + H_2$	86.5
Mg_3ReH_7	855	$^{2}/_{7}Mg_3ReH_7 \leftrightarrow {}^{6}/_{7}Mg + {}^{2}/_{7}Re + H_2$	85.4
$NaPd_3H_2$	855	$2NaPd_3H_2 \leftrightarrow 5Pd + Na_2PdH_2 + H_2$	86.5
$YbMgNiH_4$	855	$YbMgNiH_4 \leftrightarrow {}^{1}/_{3}MgNi_2 + {}^{1}/_{3}Mg_2Ni + YbH_2 + H_2$	84.9
Li_2PtH_2	840	$Li_2PtH_2 \leftrightarrow Li_2Pt + H_2$	84.4
Li_4RuH_6	840	$Li_4RuH_6 \leftrightarrow Ru + 4LiH + H_2$	83.7
Mg_3MnH_7	840	$^{2}/_{7}Mg_3MnH_7 \leftrightarrow {}^{2}/_{7}Mn + {}^{6}/_{7}Mg + H_2$	84.3
Rb_2ZnH_4	840	$^{1}/_{2}Rb_2ZnH_4 \leftrightarrow {}^{1}/_{26}RbZn_{13} + {}^{25}/_{26}Rb + H_2$	82.9
$CaMgNiH_4$	825	$CaMgNiH_4 \leftrightarrow {}^{1}/_{3}Mg_2Ni + CaH_2 + {}^{1}/_{3}MgNi_2 + H_2$	81.7
K_2ZnH_4	825	$^{25}/_{26}K_2ZnH_4 \leftrightarrow {}^{50}/_{27}KH + {}^{2}/_{27}KZn_{13} + H_2$	81.9
Li_3RhH_6	795	$Li_3RhH_6 \leftrightarrow Li_3RhH_4 + H_2$	76.2
Ca_2FeH_6	765	$Ca_2FeH_6 \leftrightarrow 2CaH_2 + Fe + H_2$	72.2
K_2PtH_6	765	$K_2PtH_6 \leftrightarrow K_2PtH4 + H_2$	70.6
Cs_2PtH_6	750	$Cs_2PtH_6 \leftrightarrow Cs_2PtH4 + H_2$	68.0
K_2ReH_9	750	$^{2}/_{7}K_2ReH_9 \leftrightarrow {}^{4}/_{7}KH + {}^{2}/_{7}Re + H_2$	69.8
Rb_2PtH_6	750	$Rb_2PtH_6 \leftrightarrow Rb_2PtH_4 + H_2$	70.1
Rb_3ZnH_5	750	$2Rb_3ZnH_5 \leftrightarrow 2Rb_2ZnH_4 + 2Rb + H_2$	69.7
Cs_3ZnH_5	735	$2Cs_3ZnH_5 \leftrightarrow 2Cs_2ZnH_4 + 2Cs + H_2$	67.8
$LiMg_2RuH_7$	735	$LiMg_2RuH_7 \leftrightarrow LiH + Mg_2RuH_4 + H_2$	67.3
Cs_3CdH_5	720	$^{2}/_{5}Cs_3CdH_5 \leftrightarrow {}^{76}/_{65}Cs + {}^{2}/_{65}Cd_{13}Cs + H_2$	64.7
Mg_2NiH_4	720	$^{1}/_{2}Mg_2NiH_4 \leftrightarrow {}^{1}/_{2}Mg_2Ni + H_2$	64.5
Mg_2RuH_6	720	$Mg_2RuH_6 \leftrightarrow Mg_2RuH_4 + H_2$	64.0
$KNaReH_9$	705	$^{4}/_{7}KNaReH_9 \leftrightarrow {}^{4}/_{7}NaH + {}^{2}/_{7}K_2ReH_9 + {}^{2}/_{7}Re + H_2$	61.7
Na_2PtH_6	690	$Na_2PtH_6 \leftrightarrow Na_2PtH4 + H_2$	59.8
Rb_3PdH_5	690	$2Rb_3PdH_5 \leftrightarrow 2Rb + 2Rb_2PdH_4 + H_2$	59.9
Cs_3PdH_5	675	$2Cs_3PdH_5 \leftrightarrow 2Cs_2PdH_4 + 2Cs + H_2$	57.9
$La_{16}Mg_8Ni_{16}H_{64}$	675	$^{1}/_{8}La_{16}Mg_8Ni_{16}H_{64} \leftrightarrow 2LaH_3 + MgNi_2 + H_2$	57.5
K_2TcH_9	660	$^{2}/_{7}K_2TcH_9 \leftrightarrow {}^{4}/_{7}KH + {}^{2}/_{7}Tc + H_2$	55.6
Na_3RuH_7	630	$^{4}/_{5}Na_3RuH_7 \leftrightarrow {}^{3}/_{5}Na_4RuH_6 + {}^{1}/_{5}Ru + H_2$	51.5
$BaReH_9$	615	$^{2}/_{7}BaReH_9 \leftrightarrow {}^{2}/_{7}Re + {}^{2}/_{7}BaH_2 + H_2$	47.1
$Li_5Pt_2H_9$	615	$^{1}/_{2}Li_5Pt_2H_9 \leftrightarrow Li_2PtH_2 + {}^{1}/_{2}LiH + H_2$	48.1
Na_2PdH_4	585	$Na_2PdH_4 \leftrightarrow Na_2PdH_2 + H_2$	43.7
$Ba_7Cu_3H_{17}$	570	$^{2}/_{3}Ba_7Cu_3H_{17} \leftrightarrow {}^{14}/_{3}BaH_2 + 2Cu + H_2$	41.2
$La_2Ni_10H_{14}$	570	$^{1}/_{7}La_2Ni_{10}H_{14} \leftrightarrow {}^{2}/_{7}LaNi_5 + H_2$	40.6
Li_2PtH_6	555	$^{1}/_{2}Li_2PtH_6\_p \leftrightarrow {}^{1}/_{2}Li_2PtH_2 + H_2$	38.8
		ternary alkaline earth (saline) metal hydrides	
Ba_2MgH_6	960	$^{17}/_{19}Ba_2MgH_6 \leftrightarrow {}^{32}/_{19}BaH_2 + {}^{1}/_{19}Ba_2Mg_{17} + H_2$	104.2
$MgSr_2H_6$	930	$MgSr_2H_6 \leftrightarrow 2SrH_2 + Mg + H_2$	98.2
Eu_2MgH_6	870	$Eu_2MgH6 \leftrightarrow 2EuH_2 + Mg + H_2$	88.1
$Ba_6Mg_7H_{26}$	840	$^{1}/_{4}Ba_6Mg_7H_{26} \leftrightarrow Mg + {}^{3}/_{4}Ba_2MgH_6 + H_2$	82.5
$SrMgH_4$	840	$2SrMgH_4 \leftrightarrow Mg + MgSr_2H_6 + H_2$	84.5
$Ba_2Mg_3H_{10}$	795	$^{3}/_{2}Ba_2Mg_3H_{10} \leftrightarrow {}^{1}/_{2}Ba_6Mg_7H_{26} + Mg + H_2$	75.3
$EuMg_2H_6$	795	$^{2}/_{3}EuMg_2H_6 \leftrightarrow {}^{1}/_{3}Eu_2MgH_6 + Mg + H_2$	76.4
$Mg_8Yb_{19}H_{54}$	750	$^{1}/_{8}Mg_8Yb_{19}H_{54} \leftrightarrow Mg + {}^{19}/_{8}YbH_2 + H_2$	69.3
$Ca_{19}Mg_8H_{54}$	735	$^{1}/_{8}Ca_{19}Mg_8H_{54} \leftrightarrow Mg + {}^{19}/_{8}CaH_2 + H_2$	66.9
$LaMg_2H_7$	735	$^{1}/_{2}LaMg_2H_7 \leftrightarrow {}^{1}/_{2}LaH_3 + Mg + H_2$	66.8

dx.doi.org/10.1021/ic501990p | Inorg. Chem. 2014, 53, 11833−11848

Table 4. Decomposition Reaction Enthalpies and Decomposition Temperatures for Binary Hydrides Studied in This Work from Experimental Sources[a]

binary hydride	T_d (K)	ΔH° [kJ mol^{-1} H_2]	$\Delta H(T)$ [kJ mol^{-1} H_2]	T [K]
YbH_2		182[c]		
LiH	993[b]	180[c]	194 (l)[c,e]	<967
	~1145[e,g]	190[e]	144 (l)[c,e]	>967
BaH_2	948[b]	177[b]		
	mp 1473			
LaH_2			208	600−1150
SrH_2	948[b]	180.3[b]	200[c]	...−1273
	mp 1323[h]	184[c]		
CaH_2	873[b]	181.5[b]	170[c]	1053−1173
	1347[g]	188[c]		
	mp 1273			
NaH	~698[b,g]	113[b]	106 (l)[c]	380−670
		112[c]		
KH	690[b]	115.4[b]	112[c]	561−688
		116[c]		
CsH	662[d]	113[d]		518−651
	443[b]	108.4[b]	112 (l)[c]	
RbH	636[f]	108.8[f]	108 (l)[c]	519−623
	443[b]	104.6[b]		
MgH_2	603[c]	75.3[b]	74[c]	713−833
	560[g]			
$PdH_{0.6}$	298[b]	40[c]		
$NiH_{0.5}$		6[c]		
$RhH_{0.5}$		−20[c]		

[a]Note: Experimentally reported values refer to heats of formation. Sign has been reversed in this table to reflect the hydrogen release reaction. melting point (mp), liquid phase (l). [b]Grochala and Edwards 2004.[4] [c]Griessen and Riesterer 1988.[100] [d]Sangster and Pelton 1994.[53] [e]Veleckis 1979.[101] [f]Sangster and Pelton 1994.[52] [g]Orecchini and Naso 2012.[102] [h]CRC Handbook.[103]

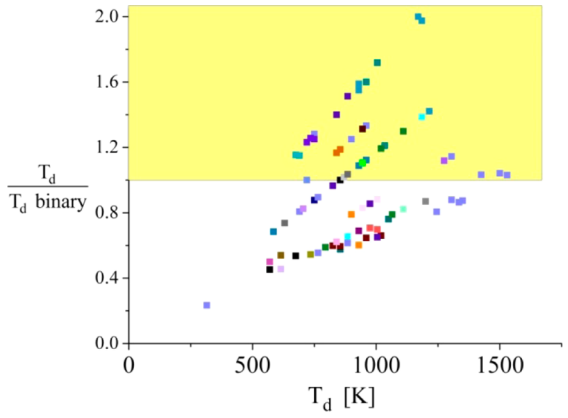

Figure 6. Relative and absolute thermal stabilities for existing ternary and quaternary CTMHs predicted with round 1 level of screening. Color indicates structure prototype. Materials in the shaded area meet the round 1 screening criterion for enhanced stability relative to the binary hydrides and are retained for round 2.

consequence of DFT calculations. In Table 5, the binary hydrides CuH, Ni−H, and MnH form only weak hydrides experimentally and will not affect the screening of desirable materials. For the Yb−H and La−H spaces, more stable binary hydride phases than those listed in Table 5 are predicted to be stable and are, thus, used in the screening. Seven of the 12 ternary CTMHs not predicted to form in the round 1 screening

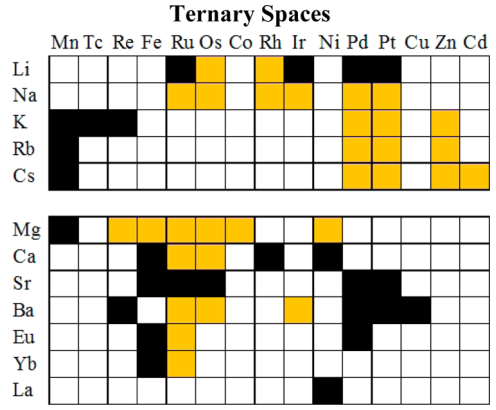

Figure 7. Ternary M−Tr−H element spaces (element combinations) studied at the round 1 level of theory that were retained (orange) and rejected (black) for round 2 screening. Element combinations are based on simulation ready CTMHs or templates from Figure 2. No quaternary M_1−M_2−Tr−H element spaces meet the enhanced stability round 1 screening criterion. Transition metals, Tr, for ternary spaces are listed horizontally. Alkali and alkaline earth metals are listed vertically for the transition metals. Element combinations not listed or shaded were not included in the overall screening.

Table 5. Existing Compounds Predicted Not to Be Thermodynamically Favored Based on Round 1 Ground State Calculations and Energies above the Stable Convex Hull

material	energy above convex hull (eV atom^{-1})	material	energy above convex hull (eV atom^{-1})
K_3ZnH_5	1.5×10^{-4}	YbH_2_	0.180
$LiMg_4Ru_2H_{13}$	3.4×10^{-4}	Eu_2PdH_4	0.201
$LaMg_2NiH_7$	8.5×10^{-4}	Cs_3PtH_5	0.233
$Mg_3Sr_2H_{10}$	9.1×10^{-3}	Rb_3PtH_5	0.240
$Ca_4Mg_3H_{14}$	5.6×10^{-3}	K_3PtH_5	0.273
$Mg_7Sr_6H_{26}$	0.012	Li_4RhH_5	0.333
$BaMgH_4$	0.013	Yb_3H_8	0.349
K_3PdH_5	0.016	LiPdH	0.375
$Yb_4Mg_3H_{14}$	0.017	Cs_3MnH_5	0.394
$EuMgH_4$	0.027	Li_4RhH_4	0.415
$Eu_6Mg_7H_{26}$	0.046	MnH	0.649
K_3MnH_5	0.050	K_3ReH_6	1.070
$Eu_2Mg_3H_{10}$	0.059	LaH_2	1.151
CuH	0.099	YbH_3	1.159
Ni_2H	0.15	Rb_3MnH_5	1.470
Ni_2H_	0.15		

will be subsequently studied at the round 2 level of theory due to the presence of a stable candidate material that meets the screening criterion that forms in the following element spaces: K−Zn−H, K−Pt−H, K−Pd−H, Cs−Pt−H, Rb−Pt−H, and Li−Rh−H. Of these seven CTMHs, five are predicted to be dynamically stabilized through vibrational effects at the higher level of theory. While it is possible that our screening methodology may overlook some materials that are stabilized through vibrational or finite temperature contributions to the free energy, only the Eu−Pd and Li−Pd systems might contain a ternary hydride that operates at the high temperatures of the NGNP and that is also more stable than the corresponding binary hydride.

Round 2. On the basis of the results from round 1, we computed the VDOS for 106 solids including 24 metals, 16 binary hydrides, 12 intermetallics, and 53 ternary CTMHs

dx.doi.org/10.1021/ic501990p | Inorg. Chem. 2014, 53, 11833−11848

listed with the relaxed structural parameters in Table S.2 in the Supporting Information. We included high temperature phases for Ca and Yb, subsequently listed as Ca_HT and Yb_HT. 1 × 1 × 1 simulation volumes were used for Cs_3PdH_3 and Rb_3PdH_3 because of the prohibitive computational expense of computing vibrational properties for the 2 × 2 × 2 supercell. Similarly, spin polarization was turned off for magnetic Mg_2Co and MgCo. On the basis of round 1 calculations, spin polarization was not required for the CTMHs studied at the round 2 level of theory. Spin polarization was turned on for Co, Fe, Ni, Pd, Ni_2H and RhH.

We predicted phase diagrams using eq 5 for P = 1 bar H_2 and $0 \leq T$ (K) ≤ 2000, accounting for the vibrational Helmholtz free energy of the condensed phases. This constitutes our best estimate of the relative and absolute thermodynamic stabilities of candidate CTMHs. The stabilities of the 51 stable CTMHs are shown in Figure 8. Only Li_4RhH_5, Rb_3PdH_3, and Rb_3PtH_5

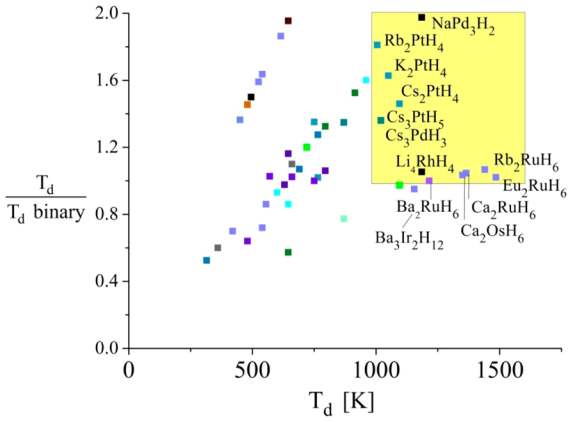

Figure 8. Relative and absolute thermal stabilities for the reduced set of existing ternary CTMHs predicted with round 2 level of screening. Color indicates structure prototype. Materials in the shaded area are the final candidates that meet the round 2 screening criteria for both enhanced stability relative to the binary hydrides and $T_d \geq 1000$ K.

are not predicted to form at any temperature. In each of these element spaces, a stable CTMH of a different composition forms. As shown in Figure 8, 13 CTMHs meet both screening criteria, that is, they have $T_d/T_{d,binary} \geq 1$ and $T_d \geq 1000$ K. The final candidates are listed in Table 6 in order of highest hydrogen release temperature. The top five materials crystallize in the 2−Sr_2RuH_6 cubic crystal structure, and three others crystallize with the 6−K_2PtH_4 tetragonal prototype. In both of these examples, the cations adopt 8-fold cubic or nearly cubic arrangements, which Yvon and Renaudin argue may help maximize the M−H interactions, stabilizing the structures.[43] In the case of the 6−K_2PtH_4 prototype, there is evidence that the low temperature form studied in this work transforms to a disordered cubic structure similar to that of 2−Sr_2RuH_6 near ambient conditions.[43]

It is notable that, of the 13 final candidates, 11 crystallize in either cubic or tetragonal symmetry, and most have high temperature disordered cubic phases. Since disordered phases are not studied in this work and the high temperature modifications, if thermodynamically stable, are expected to have lower free energies than the ordered materials, the T_d values reported here may be taken as lower bounds if one ignores the potential existence of other destabilizing intermetallic phases. Of the most stable element spaces from Table 6, only binary intermetallics RuYb, LiRh, and Cs_2Pt are listed in the ICSD as known compounds. Therefore, the most stable CTMHs decompose to the pure metal phases and hydrogen, existing in element combinations in which the two constituent metals do not favor forming ordered intermetallics. This is a somewhat general feature of CTMHs as discussed earlier since most CTMHs are true ternary compounds, that is, they do not form via hydrogen dissolution into an intermetallic lattice.[43]

Table S.3 in the Supporting Information presents key computed thermodynamic properties for the binary hydrides relevant for the round 2 level of screening. Calculated values for enthalpy and entropy include temperature-dependent and zero point vibrational contributions for the condensed phases. These are directly computed values rather than linearly fit values and can be compared with the experimental reference data in Table 4. The experimental data are typically retrieved from van't Hoff plots generated from averages of measured pressures from pressure−composition isotherms and absolute agreement between experiment and DFT values should not be expected. In general, the calculations reproduce the increase in reaction enthalpy from 300 K to the high temperature reaction conditions due to inclusion of the temperature-dependent vibrational enthalpy. In most cases the DFT predicts T_d to within 125 K of the experimental value where available. This is

Table 6. Final Candidates from Round 2 Screening with $T_d/T_{d,binary} \geq 1$ and $T_d \geq 1000$ K[a]

CTMH	T_d (K)	decomposition pathway	structure prototype
Eu_2RuH_6	1485	$^1/_3Eu_2RuH_6 \leftrightarrow {}^2/_3Eu + {}^1/_3Ru + H_2$	2−Sr_2RuH_6
Yb_2RuH_6	1440	$^1/_3Yb_2RuH_6 \leftrightarrow {}^1/_3Ru + {}^2/_3Yb\_HT + H_2$	2−Sr_2RuH_6
Ca_2RuH_6	1365	$^1/_3Ca_2RuH_6 \leftrightarrow {}^2/_3Ca\_HT + {}^1/_3Ru + H_2$	2−Sr_2RuH_6
Ca_2OsH_6	1350	$^1/_3Ca_2OsH_6 \leftrightarrow {}^2/_3Ca\_HT + {}^1/_3Os + H_2$	2−Sr_2RuH_6
Ba_2RuH_6	1215	$^1/_3Ba_2RuH_6 \leftrightarrow {}^2/_3Ba + {}^1/_3Ru + H_2$	2−Sr_2RuH_6
$Ba_3Ir_2H_{12}$	1215	$i^1/_6Ba_3Ir_2H_{12} \leftrightarrow {}^1/_2Ba + {}^1/_3Ir + H_2$	31−$Ba_3Ir_2H_{12}$
Li_4RhH_4	1185	$^1/_2Li_4RhH_4 \leftrightarrow {}^1/_2LiRh + {}^3/_2Li + H_2$	Li_4RhH_4
$NaPd_3H_2$	1185	$NaPd_3H_2 \leftrightarrow 3Pd + Na + H_2$	$NaPd_3H_2$
Cs_2PtH_4	1095	$^1/_2Cs_2PtH_4 \leftrightarrow {}^1/_2Cs_2Pt + H_2$	6−K_2PtH_4
K_2PtH_4	1050	$^1/_2K_2PtH_4 \leftrightarrow K + {}^1/_2Pt + H_2$	6−K_2PtH_4
Cs_3PtH_5	1020	$2Cs_3PtH_5 \leftrightarrow 2Cs_2PtH_4 + 2Cs + H_2$	8−K_3PtH_5
Cs_3PdH_3	1020	$^2/_3Cs_3PdH_3 \leftrightarrow 2Cs + {}^2/_3Pd + H_2$	9−K_3PdH_3
Rb_2PtH_4	1005	$^1/_2Rb_2PtH_4 \leftrightarrow {}^1/_2Pt + Rb + H_2$	6−K_2PtH_4

[a]Decomposition reactions, hydrogen release temperatures for 1 bar H_2, and structure prototype are shown.

dx.doi.org/10.1021/ic501990p | Inorg. Chem. 2014, 53, 11833−11848

consistent with our previous thermodynamic stability calculations of very stable binary hydrides.[26] There are larger uncertainties for CaH_2 and BaH_2 for which the experimental data are ambiguous. LiH melts before releasing hydrogen, and so we also list the melting temperatures of the most stable binary hydrides for CaH_2 and BaH_2 as perhaps a better indicator of the thermodynamic stability compared to the values reported in ref 4.

The average value of the ambient condition reaction entropy is 0.134 kJ K^{-1} mol H_2, very close to the entropy of the H_2 gas at 0.130 kJ K^{-1} mol^{-1} H_2. However, $\Delta S°$ is calculated to fall between 0.098 and 0.185 kJ K^{-1} mol^{-1} H_2, a large spread. From the recommended values for $\Delta G°$ from Sangster and Pelton, the experimental value of $\Delta S°$ is 0.171 and 0.170 kJ K^{-1} mol^{-1} H_2 for RbH and CsH, respectively. This is, clearly, much larger than the standard entropy of H_2 gas. Our calculations predict smaller values for RbH and CsH at 0.153 and 0.116 kJ K^{-1} mol^{-1} H_2, respectively. In general, we note that the dihydride binary hydrides have computed values of $T\Delta S°$ at 300 K (40.6 ± 0.8 kJ mol^{-1} H_2) closer to the ideal entropic contribution of H_2 gas of 39.0 kJ mol^{-1} H_2, than the monohydrides (40.0 ± 6.3 kJ mol^{-1} H_2) for which the scatter is larger.

Table 7 summarizes the thermodynamic properties for the hydrogen release reactions of final candidate materials from Table 6 as a result of the round 2 screening. We note the very large thermodynamic driving force for hydrogen in the solid hydride for these materials, characterized by the reaction enthalpy. As with the binary hydride CsH, $\Delta S°$ for the Cs−Pd and Cs−Pt hydrides are significantly reduced compared with the entropy of hydrogen gas and the other CTMHs. There are very few experimental thermodynamic data available for the CTMHs, a point which highlights the utility of computational tools. However, we compare our results with experimental phase stability observations for a few examples below.

Table 7. Thermodynamic Properties of Final Candidate Decomposition Reactions from Table 6 from Round 2 Calculations, Including Vibrational Corrections to the Helmholtz Free Energy for Condensed Phases[a]

CTMH	$\Delta H°$	$\Delta S°$	$\Delta H(T_d)$
Eu_2RuH_6	196.7	0.131	189.5
Yb_2RuH_6	192.1	0.132	185.9
Ca_2RuH_6	180.8	0.131	175.0
Ca_2OsH_6	179.0	0.130	173.8
Ba_2RuH_6	159.7	0.130	154.7
$Ba_3Ir_2H_{12}$	153.2	0.124	150.0
Li_4RhH_4	165.6	0.138	161.9
$NaPd_3H_2$	124.1	0.111	111.4
Cs_2PtH_4	133.6	0.123	128.5
K_2PtH_4	141.2	0.133	139.4
Cs_3PtH_5	63.9	0.075	44.5
Cs_3PdH_3	114.0	0.116	104.5
Rb_2PtH_4	136.8	0.134	135.3

[a]Standard conditions (300 K, 1 bar H_2). T_d (K), ΔH (kJ mol^{-1} H_2), $\Delta S°$ (kJ K^{-1} mol^{-1} H_2).

Comparison of Experimental and Predicted Phase Diagrams. As previously mentioned, the most well-studied CTMH system is the Mg−Fe−H system element space.[17,47−49] Puszkiel et al. measured pressure−composition isotherms using a modified Sieverts type apparatus.[49] They found that the ternary hydride exhibits lower hydrogen equilibrium pressure than the binary hydride for the same temperature, indicating higher ternary hydride thermodynamic stability. Based on pressures determined through averages of experimental points and van't Hoff plot fitting, they determined characteristic thermodynamic properties for Mg_2FeH_6 of $T_d \approx 580$ K, $\Delta H(573-648\ K) = 80 \pm 7$ kJ mol^{-1} H_2, and $\Delta S = 0.137 \pm 13$ kJ K^{-1} mol^{-1} H_2 and for MgH_2 of $T_d \approx 540$ K, $\Delta H(548-648$ K) = 67 ± 2 kJ mol^{-1} H_2, and $\Delta S = 0.123 \pm 3$ kJ K^{-1} mol^{-1} H_2. More directly, Polanski et al., who determined T_d for the direct decomposition of Mg_2FeH_6 to the elements using differential scanning calorimetry measurements under 1 bar H_2 overpressure, reported onset and peak temperatures of 650 and 693 K, respectively, and ΔH = 65.6 kJ mol^{-1} H_2.[51] Similarly, Bogdanovic et al. found the ΔH (Mg_2FeH_6) = 77 kJ mol^{-1} H_2.[17] For comparison, our predictions from the round 2 level screening calculations are shown in Table 8. We reproduce the enhanced stability of the CTMH, both in terms of the relative stability with respect to the binary hydride and magnitude of the onset of hydrogen release temperatures. The predicted decomposition pathway and thermodynamic properties are in good agreement with the experimental values.

Table 8. Predicted Thermodynamic Properties for Mg−Fe−H System

CTMH	binary
$^1/_3Mg_2FeH_6 \leftrightarrow {}^2/_3Mg + {}^1/_3Fe + H_2$	$MgH_2 \leftrightarrow Mg + H_2$
T_d = 660 K	T_d = 480 K
$\Delta H(T_d)$ = 86.2 kJ mol^{-1} H_2	$\Delta H(T_d)$ = 62.4 kJ mol^{-1} H_2
$\Delta S°$= 0.127 kJ K^{-1} mol^{-1} H_2	$\Delta S°$= 0.131 kJ K^{-1} mol^{-1} H_2

Though not as well studied, the thermal stabilities of M_2ZnH_4 and M_3ZnH_5 ternary hydrides (M = K, Rb, and Cs) have been investigated via thermogravimetry methods.[104,105] Borst, Hewat, and Yvon found that all of the ternary compounds decomposed around 600 K at ambient pressures.[105] For M_2ZnH_4, the M = K and Rb compounds begin to decompose to a mixture of the binary intermetallic MZn_{13} and M_3ZnH_5 phases at 550 and 580 K, respectively, and they attribute a second decomposition step to formation of the binary hydrides at 637 and 680 K, respectively. Cs_2ZnH_4 releases hydrogen in one step.[104] For M_3ZnH_5 (M = K, Rb, and Cs), the hydrides release hydrogen at 620, 630, and 625 K, respectively. However, it is uncertain as to whether or not the hydride decomposes to the pure metals or to a mixture of the binary hydrides and intermetallic phases.[105]

Figure 9 shows our phase diagram predictions for these systems, including vibrational corrections to the Helmholtz free energies. We calculate that the ternary hydrides all decompose in the range 570 K−795 K and that each is at least as, if not slightly more, thermodynamically stable than the binary hydride in each system. For the K−Zn−H system, the thermodynamically preferred decomposition path for K_2ZnH_4 is through a mixture of K_3ZnH_4 and KZn_{13}, in agreement with the experimental observation. However, the relative stabilities of the CTMH are reversed for the Rb−Zn−H system. In both cases, the binary intermetallic phase is stable. Additionally, we find that Cs_2ZnH_4 releases hydrogen in one step, also in agreement with the experimental observation.

In computing the phase diagrams, we increment the hydrogen chemical potential by an amount equivalent to ΔT = 15 K, which sets one level of tolerance for the precision of the reported reaction temperatures. In this work, attempts have

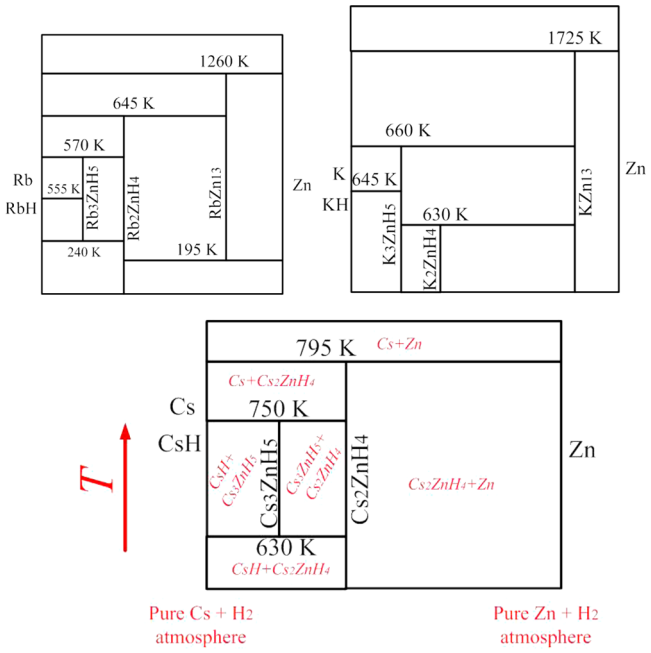

Figure 9. Predicted phase diagrams at 1 bar H_2 for the *M*−Zn−H (*M* = Rb, K, and Cs) systems with vibrational contributions for the condensed phases (not drawn to scale). The horizontal axis represents the molar ratio of metals for a given composition with the pure cation species on the far left and the pure transition metal on the far right. Temperature is shown vertically. As demonstrated for the Cs−Zn−H element space, each box describes a unique mixture of stable compounds. The stable mix of compounds obtained from the GCLP method for a given *T* can be read from the intersection of a horizontal line drawn at that *T* with the vertical lines, which represent the stoichiometric compounds.

been made to control numerical convergence of compound free energies with respect to *k*-points, cutoff energy, supercell size, and *q*-point sampling to within approximately 5 kJ mol^{-1} (kJ mol^{-1} H_2 for hydride phases). One expects that there will be some cancellation of errors when considering relative phase stabilities, particularly with respect to the cutoff energy. A larger issue is the accuracy of the DFT functionals themselves. Comparing the DFT computed and experimental heats of reaction for the binary hydrides in Tables 4 and S.3 (in the Supporting Information) suggests that the PAW(GGA,PW91) pseudopotential used in this work can be expected to resolve reaction enthalpies either at ambient conditions or at the reaction temperature to within about 15 kJ mol^{-1} H_2 (on average) of the experimental reference value. However, deviations can be as large as 30 kJ mol^{-1} H_2 as is the case for CsH. This is consistent with the results of Wolverton et al., who found that the average root-mean-square error for computing dehydrogenation enthalpies at 298 K decreases from 19.4 to 14.7 kJ mol^{-1} H_2 when accounting for vibrational effects in Perdew−Wang GGA DFT calculations, similar to those used in this paper.[9] Based on the average error ($\Delta H_{expt} - \Delta H_{DFT}$) = 15 kJ $mol^{-1}H_2$ and the average $\Delta S°$ = 0.125 kJ K^{-1} mol^{-1} H_2, we estimate that the absolute magnitudes of decomposition temperatures are typically accurate to within about 125 K. We expect that the relative magnitudes of binary and ternary hydrides are even better reproduced because of some cancellation of exchange-correlation effect errors. Therefore, the phase diagrams predicted in this work should be taken as guides rather than as absolute answers. Phase diagrams for the element spaces of the final candidate materials listed in Table 6 are available in Figure S.5 in the Supporting Information. The calculations can clearly sort metal hydrides that have low, moderate, and high thermal stabilities and are useful for determining potential operating parameters of candidate systems for the NGNP and other high temperature applications.

Dynamically Stabilized Compounds. Some element spaces have significant changes in the predicted stable sets of compounds for given chemical potentials from round 1 to round 2, which incorporate the vibrational contributions to the free energy for the condensed phases. Notable differences include the stabilization of Li_4RhH_4 at 705 K via the reaction of LiH and Li_3RhH_4 as shown in Supporting Information Figure S.5 g and, upon heating, Li_3RhH_4 phase separates into the intermetallic LiRh and Li_4RhH_4. This is a significant change from the phase diagram calculated based only on ground state energies for which Li_4RhH_4 was not predicted to form at any *T*. Other significant changes include the dynamic stabilization of K_3PtH_5, K_3PdH_5, K_3ZnH_5, Cs_3PdH_5, Cs_3PtH_5, and K_3ZnH_5 with corresponding change in the decomposition of K_2ZnH_4 ($^{76}/_{27}K_2ZnH_4 \leftrightarrow {}^{50}/_{27}K_3ZnH_5 + {}^{2}/_{27}KZn_{13} + H_2$), the destabilization of Rb_3PdH_3 with corresponding change in decomposition of Rb_2PdH_4 ($^{1}/_{2}Rb_2PdH_4 \leftrightarrow Rb + {}^{1}/_{2}Pd + H_2$), and the flip-flop of relative stabilities of Na_2PdH_2 ($^{3}/_{2}Na_2PdH_2 \leftrightarrow {}^{5}/_{2}Na + {}^{1}/_{2}NaPd_3H_2 + H_2$) and $NaPd_3H_2$ ($NaPd_3H_2 \leftrightarrow 3Pd + Na + H_2$).

Final Candidate van't Hoff Plots. Figures 10 and 11 show the computed van't Hoff plots for the final candidate CTMHs and the binary hydrides using eq 8 to correct the hydrogen chemical potential for pressure. The screening criteria were sufficient to ensure that the CTMHs in Figure 10 are at least as stable as the corresponding binary hydrides at the pressure conditions studied in this work from $P = 10^{-6}$ to 100 bar. At *T* = 1000 K, the most thermodynamically stable CTMHs are, in order from highest to lowest, Eu_2RuH_6, Yb_2RuH_6, Ca_2RuH_6, Ca_2OsH_6, and Ba_2RuH_6, which are all materials that crystallize in the 2−Sr_2RuH_6 cubic prototype. These represent the most stable CTMH materials with enhanced stability with respect to the associated binary hydrides.

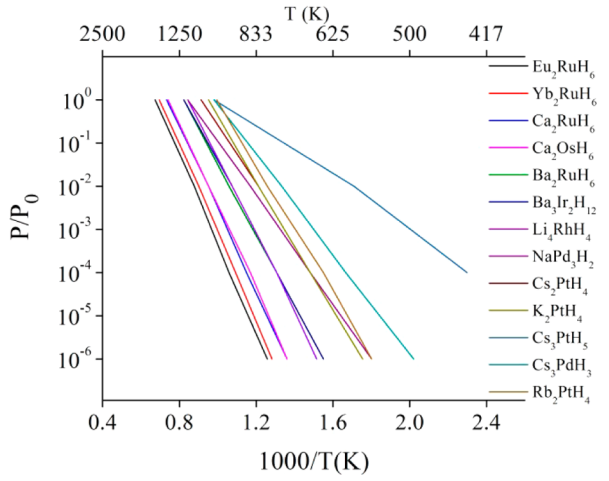

Figure 10. Calculated van't Hoff plots for final candidate CTMHs from Table 6 based on the round 2 level of screening.

Tritium Gettering for the NGNP Application. The conditions of the NGNP will contain low levels of tritium

dx.doi.org/10.1021/ic501990p | Inorg. Chem. 2014, 53, 11833−11848

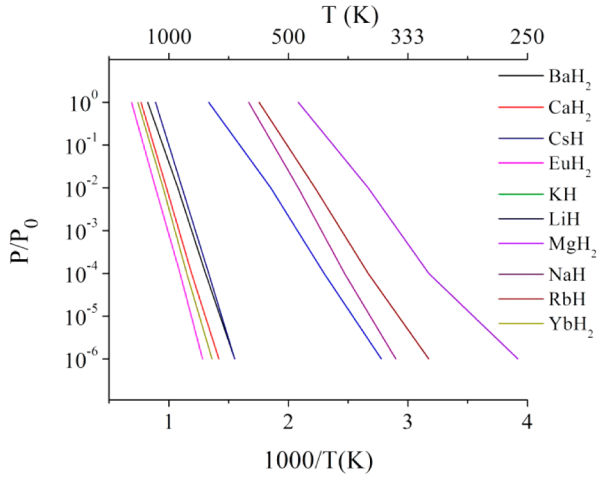

Figure 11. Calculated van't Hoff plots for binary hydrides corresponding to materials in Table 6 based on the round 2 level of screening.

contamination, for example, 10^{-10} bar H_2.[106] The most stable predicted ternary hydride, Eu_2RuH_6, has an equilibrium pressure of $\sim 10^{-4}$ bar at the NGNP condition T = 1000 K. A less expensive binary hydride, CaH_2, is calculated to have P_{eq} (1000 K) $\approx 10^{-2}$ bar. Both of the most stable binary and ternary hydrides studied here have equilibrium pressures far above that of the target tritium contaminant. This implies that there will be a significant thermodynamic driving force for tritium to remain in the gas phase rather than form the solid hydride material at the temperature conditions of the NGNP.

One arrangement of the tritium gettering system could use a direct contact bed that exposes the metal hydriding material to a side stream of the helium coolant and tritium contaminant at the reactor outlet temperatures. This has the advantage of greater thermal efficiency since the coolant is not being cooled, and the gettering bed can be placed far upstream of other processing equipment to limit contamination of equipment such as heat exchangers. However, this arrangement will suffer from the thermodynamic drawback discussed above. Some processing options to enable the use of CTMHs for the gettering process could include raising the H_2 partial pressure. H_2 as protium will be present in the helium coolant in addition to tritium but at levels that are currently unknown. However, since tritium and protium have very similar thermodynamic stabilities in metal hydrides at high temperature, this may increase the amount of tritium taken up by the direct contact bed. Additionally, H_2 injection into the side stream could be considered. H_2 injection is being investigated for the NGNP as a method for raising the backpressure on heat exchangers to prevent tritium migration to downstream users.[24] Raising P_{H_2} moves the equilibrium point for CTMH candidates in Figure 10 to the left, meaning that the material will absorb H_2 at higher temperatures. On the basis of the most thermodynamically stable CTMH candidate, Eu_2RuH_6, the P_{H_2} would need to be raised to above $\sim 10^{-3}$ bar to make the hydriding reaction energetically favorable. As the amount of hydrogen in the coolant increases, the overall system will require more metal hydride material to accommodate the additional gas to be stored.

Other options could include cooling the side stream to move the equilibrium point for CTMHs to lower partial pressures on the van't Hoff plots. This would lower the thermodynamic driving force for hydrogen to remain in the gas phase, but would also cost energy and require tritium management materials to cool the stream, though some heat may be recoverable via the exothermic hydriding reaction.

CONCLUSIONS

Our DFT calculations and GCLP phase diagram prediction methods reproduce experimental trends in phase stability with reasonable fidelity and be can considered as a guide for ranking metal hydrides based on hydrogen release temperatures at 1 bar H_2 to within ~125 K. Using two rounds of screening, we successfully identified 13 candidate CTMHs from an initial library of 102 ternary and quaternary CTMHs that have the desirable properties of enhanced thermodynamic stability relative to the associated binary hydrides and that release hydrogen at high temperature for 1 bar H_2 overpressures. The most stable CTMHs tend to crystallize in the 2−Sr_2RuH_6 cubic prototype structure and decompose to the pure elements and hydrogen rather than to intermetallic phases. Unfortunately, all of the 13 candidate CTMHs that result from our analysis include elements that are relatively expensive, a fact that may strongly limit use of these materials in practical applications.

A limitation of our results is that we considered only materials that do not exhibit partial occupancies. If future efforts are made to refine computational predictions for CTMHs at high temperatures, it would be useful to expand our current results by incorporating algorithms that can explore the diversity of structures that can occur in materials with partial occupancies. We note that materials of this kind are potentially important at elevated temperatures because under these conditions the configurational entropy associated with disordered sites can make a nonnegligible contribution to the overall free energy.

We have significantly expanded the available thermodynamic properties of CTMH systems. Our computed characteristic T_d values, enthalpies and entropies of formation, van't Hoff plots, and phase diagrams may be used as a guide for selecting high temperature CTMHs for a given application. We also observed the dynamic stabilization of some CTMH compositions (~10) with the inclusion of vibrational free energies in the GCLP phase diagram prediction, which illustrates the necessity of including such corrections in the calculation of the relative phase stabilities of compounds in multicomponent systems. The most stable CTMHs and calculated binary hydrides are predicted to have equilibrium pressures orders of magnitude above the tritium contaminant levels of the NGNP application. On the basis of the ideal thermodynamic considerations of the very stable metal hydrides considered here, there are significant challenges to using binary hydrides or CTMHs in a direct contact gettering application at high temperature and low tritium overpressures. Process manipulations should be considered that either increase the hydrogen overpressure in the system or that cool the feed streams in order to drive the thermodynamic equilibrium in favor of the solid metal hydrides.

ASSOCIATED CONTENT

Supporting Information

Listings are available of the studied materials lattice parameters computed at round 1 and round 2 levels of theory, convergence testing details, as well as phase diagrams for final candidates. This material is available free of charge via the Internet at http://pubs.acs.org.

AUTHOR INFORMATION

Corresponding Author

*E-mail: david.sholl@chbe.gatech.edu.

Notes

The authors declare no competing financial interest.

ACKNOWLEDGMENTS

This research was performed using funding received from the DOE Office of Nuclear Energy's Nuclear Energy University Programs

REFERENCES

(1) Zhou, L. *Renewable Sustainable Energy Rev.* **2005**, *9*, 395−408.
(2) Schlapbach, L.; Zuttel, A. *Nature* **2001**, *414*, 353−358.
(3) Züttel, A. *Mater. Today* **2003**, *6*, 24−33.
(4) Grochala, W.; Edwards, P. P. *Chem. Rev.* **2004**, *104*, 1283−1316.
(5) Sakintuna, B.; Lamari-Darkrim, F.; Hirscher, M. *Int. J. Hydrogen Energy* **2007**, *32*, 1121−1140.
(6) Alapati, S. V.; Johnson, J. K.; Sholl, D. S. *J. Phys. Chem. C* **2008**, *112*, 5258−5262.
(7) Alapati, S. V.; Johnson, J. K.; Sholl, D. S. *Phys. Chem. Chem. Phys.* **2007**, *9*, 1438−1452.
(8) Kim, K. C.; Sholl, D. S. *J. Phys. Chem. C* **2009**, *114*, 678−686.
(9) Wolverton, C.; Donald, J. S.; Akbarzadeh, A. R.; Ozoliņš, V. *J. Phys.: Condens. Matter* **2008**, *20*, No. 064228.
(10) van Houten, R.; Bartram, S. *Metall. Trans.* **1971**, *2*, 527−530.
(11) Bartscher, W.; Rebivant, J.; Boeuf, A.; Caciuffo, R.; Rustichelli, F.; Fournier, J. M.; Kuhs, W. F. *J. Less-Common Met* **1986**, *121*, 455−460.
(12) Terrani, K. A.; Chinthaka Silva, G. W.; Yeamans, C. B.; Balooch, M.; Olander, D. R. *J. Nucl. Mater.* **2009**, *392*, 151−157.
(13) Konashi, K.; Pudjanto, B. A.; Terai, T.; Yamawaki, M. *J. Phys. Chem. Solids* **2005**, *66*, 625−628.
(14) Bartscher, W.; Rebizant, J.; Haschke, J. M. *J. Less-Common Met.* **1988**, *136*, 385−394.
(15) Zhu, W.; Wang, R.; Shu, G.; Wu, P.; Xiao, H. *J. Phys. Chem. C* **2010**, *114*, 22361−22368.
(16) Simnad, M. T. *Nucl. Eng. Des.* **1981**, *64*, 403−422.
(17) Bogdanović, B.; Reiser, A.; Schlichte, K.; Spliethoff, B.; Tesche, B. *J. Alloys Compd.* **2002**, *345*, 77−89.
(18) Felderhoff, M.; Bogdanović, B. *Int. J. Mol. Sci.* **2009**, *10*, 325−344.
(19) Gil, A.; Medrano, M.; Martorell, I.; Lázaro, A.; Dolado, P.; Zalba, B.; Cabeza, L. F. *Renewable Sustainable Energy Rev.* **2010**, *14*, 31−55.
(20) Harries, D. N.; Paskevicius, M.; Sheppard, D. A.; Price, T. E. C.; Buckley, C. E. *Proc. IEEE* **2012**, *100*, 539−549.
(21) U.S. DOE Nuclear Energy Research Advisory Committee and Generation IV International Forum. *A Technology Roadmap for Generation IV Nuclear Energy Systems*. Report Number 03-GA50034; U.S. DOE: Washington, DC, 2002.
(22) U.S. DOE Office of Nuclear Energy. *Next Generation Nuclear Plant Report to Congress*; U.S. DOE: Washington, DC, 2010.
(23) U.S. DOE. *The U.S. Generation-IV Implementation Strategy*. DOE Office of Nuclear Energy: Washington, DC, 2003.
(24) Sherman, S. R.; Adams, T. M. *Tritium Barrier Materials and Separation Systems for the NGNP*; Savannah River National Laboratory: Aiken, SC, 2008.
(25) NGNP Project. *Next Generation Nuclear Plant Project: Preliminary Project Plan*; Idaho National Laboratory: Idaho Falls, ID, 2007.
(26) Nicholson, K. M.; Sholl, D. S. *Phys. Rev. B* **2012**, *86*, No. 134113.
(27) Nicholson, K. M.; Sholl, D. S. *J. Chem. Eng. Data* **2014**, in press.
(28) Bouten, P. C. P.; Miedema, A. R. *J. Less-Common Met.* **1980**, *71*, 147−160.
(29) George, L.; Hrubiak, R.; Rajan, K.; Saxena, S. K. *J. Alloys Compd.* **2009**, *478*, 731−735.
(30) Miwa, K.; Fukumoto, A. *Phys. Rev. B* **2002**, *65*, 155114.
(31) Smithson, H.; Marianetti, C. A.; Morgan, D.; Van der Ven, A.; Predith, A.; Ceder, G. *Phys. Rev. B* **2002**, *66*, 144107.
(32) Xu, Q.; Van der Ven, A. *Phys. Rev. B* **2007**, *76*.
(33) Wagner, L. K.; Majzoub, E. H.; Allendorf, M. D.; Grossman, J. C. *Phys. Chem. Chem. Phys.* **2012**, *14*, 6611−6616.
(34) Khatamian, D.; Manchester, F. D. *J. Phase Equilib.* **1988**, *9*, 252−260.
(35) Bashkin, I. O.; Ponyatovskii, E. G.; Kost, M. E. *Phys. Status Solidi B* **1978**, *87*, 369−372.
(36) Buschow, K. H. J.; Bouten, P. C. P.; Miedema, A. R. *Rep. Prog. Phys.* **1982**, *45*, 937−1039.
(37) Sandrock, G.; Thomas, G. *Appl. Phys. A: Mater. Sci. Process.* **2001**, *72*, 153−155.
(38) Beck, R. L.; Mueller, W. M. Zirconium Hydrides and Hafnium Hydrides. In *Metal Hydrides*; Academic Press: New York, 1968; p 241.
(39) Sangster, J.; Pélton, A. D. *J. Phase Equilib.* **1993**, *14*, 373−381.
(40) Mueller, W. M. Titanium Hydrides. In *Metal Hydrides*; Academic Press: New York, 1968; p 336.
(41) Libowitz, G. G. The Actinide Hydrides. In *Metal Hydrides*; Mueller, W. M., Blackledge, J. P., Libowitz, G. G., Eds.; Academic Press: New York, 1968; p 490.
(42) *DOE Handbook: Tritium Handling and Safe Storage*; U.S. Department of Energy: Washington, D.C., 1999.
(43) Yvon, K.; Renaudin, G. Hydrides: Solid State Transition Metal Complexes. In *Encyclopedia of Inorganic Chemistry*, 2nd ed.; King, B. R., Ed.; John Wiley & Sons: Chichester, U.K., 2005; Vol. III, pp 1814−1846.
(44) Bogdanović, B.; Sandrock, G. *MRS Bull.* **2002**, *27*, 712−716.
(45) Griessen, R.; Driessen, A. *J. Less-Common Met.* **1984**, *103*, 245−257.
(46) Miedema, A. R.; Buschow, K. H. J.; Van Mal, H. H. *J. Less-Common Met* **1976**, *49*, 463−472.
(47) Didisheim, J. J.; Zolliker, P.; Yvon, K.; Fischer, P.; Schefer, J.; Gubelmann, M.; Williams, A. F. *Inorg. Chem.* **1984**, *23*, 1953−1957.
(48) George, L.; Drozd, V.; Durygin, A.; Chen, J.; Saxena, S. K. *Int. J. Hydrogen Energy* **2009**, *34*, 3410−3416.
(49) Puszkiel, J. A.; Larochette, P. A.; Gennari, F. C. *J. Alloys Compd.* **2008**, *463*, 134−142.
(50) Miwa, K.; Takagi, S.; Matsuo, M.; Orimo, S. *J. Phys. Chem. C* **2013**, *117*, 8014−8019.
(51) Polanski, M.; Nielsen, T. K.; Cerenius, Y.; Bystrzycki, J.; Jensen, T. R. *Int. J. Hydrogen Energy* **2010**, *35*, 3578−3582.
(52) Sangster, J.; Pélton, A. D. *J. Phase Equilib.* **1994**, *15*, 87−89.
(53) Sangster, J.; Pélton, A. D. *J. Phase Equilib.* **1994**, *1*, 84−86.
(54) Akbarzadeh, A. R.; Ozoliņš, V.; Wolverton, C. *Adv. Mater.* **2007**, *19*, 3233−3239.
(55) Michel, K. J.; Akbarzadeh, A. R.; Ozolins, V. *J. Phys. Chem. C* **2009**, *113*, 14551−14558.
(56) Kim, K. C.; Kulkarni, A. D.; Johnson, J. K.; Sholl, D. S. *Phys. Chem. Chem. Phys.* **2011**, *13*, 7218−7229.
(57) Akbarzadeh, A. R.; Wolverton, C.; Ozolins, V. *Phys. Rev. B* **2009**, *79*, 184102.
(58) Majzoub, E. H.; Zhou, F.; Ozoliņš, V. *J. Phys. Chem. C* **2011**, *115*, 2636−2643.
(59) Ong, S. P.; Wang, L.; Kang, B.; Ceder, G. *Chem. Mater.* **2008**, *20*, 1798−1807.
(60) Parker, S. F. *Coord. Chem. Rev.* **2010**, *254*, 215−234.
(61) FIZ Karlsruhe. *The Inorganic Crystal Structure Database (ICSD)*. http://www.fiz-karlsruhe.de/icsd.html.
(62) Bergerhoff, G.; Brown, I. D. In *Crystallographic Databases*; Allen, F. H., Bergerhoff, G., Severs, R., Eds.; International Union of Crystallography: Chester, U.K., 1987.
(63) Nakamori, Y.; Miwa, K.; Ninomiya, A.; Li, H.; Ohba, N.; Towata, S.-i.; Züttel, A.; Orimo, S.-i. *Phys. Rev. B* **2006**, *74*, No. 045126.

(64) Miwa, K.; Aoki, M.; Noritake, T.; Ohba, N.; Nakamori, Y.; Towata, S.; Züttel, A.; Orimo, S. *Phys. Rev. B* **2006**, *74*, No. 155122.
(65) Miwa, K.; Ohba, N.; Towata, S.; Nakamori, Y.; Züttel, A.; Orimo, S. *J. Alloys Compd.* **2007**, *446*−*447*, 310−314.
(66) Alapati, S. V.; Johnson, J. K.; Sholl, D. S. *J. Phys. Chem. B* **2006**, *110*, 8769−8776.
(67) Alapati, S. V.; Johnson, J. K.; Sholl, D. S. *J. Phys. Chem. C* **2007**, *111*, 1584−1591.
(68) Wolverton, C.; Ozoliņš, V. *Phys. Rev. B* **2007**, *75*, No. 064101.
(69) Ozolins, V.; Akbarzadeh, A. R.; Gunaydin, H.; Michel, K.; Wolverton, C.; Majzoub, E. H. *J. Phys. Conf. Ser.* **2009**, *180*, No. 012076.
(70) Kim, K. C.; Kulkarni, A. D.; Johnson, J. K.; Sholl, D. S. *Phys. Chem. Chem. Phys.* **2011**, *13*, 21520−21529.
(71) Yong-li, W.; Shi, L.; Li-jian, R.; Yuan-ming, W. *J. Phys.: Condens. Matter* **2010**, *22*, No. 175502.
(72) Hummelshøj, J. S.; Landis, D. D.; Voss, J.; Jiang, T.; Tekin, A.; Bork, N.; Dułak, M.; Mortensen, J. J.; Adamska, L.; Andersin, J.; et al. *J. Chem. Phys.* **2009**, *131*, No. 014101.
(73) Chen, J.; Kuriyama, N.; Xu, Q.; Takeshita, H. T.; Sakai, T. *J. Phys. Chem. B* **2001**, *105*, 11214−11220.
(74) Li, D.; Zhang, T.; Yang, S.; Tao, Z.; Chen, J. *J. Alloys Compd.* **2011**, *509*, 8228−8234.
(75) Parker, S. F.; Bennington, S. M.; Ramirez-Cuesta, A. J.; Auffermann, G.; Bronger, W.; Herman, H.; Williams, K. P. J.; Smith, T. *J. Am. Chem. Soc.* **2003**, *125*, 11656−11661.
(76) Parker, S. F.; Refson, K.; Williams, K. P. J.; Braden, D. A.; Hudson, B. S.; Yvon, K. *Inorg. Chem.* **2006**, *45*, 10951−10957.
(77) Kohlmann, H.; Moyer, R. O., Jr; Hansen, T.; Yvon, K. *J. Solid State Chem.* **2003**, *174*, 35−43.
(78) Moyer, R. O., Jr; Antao, S. M.; Toby, B. H.; Morin, F. G.; Gilson, D. F. R. *J. Alloys Compd.* **2008**, *460*, 138−141.
(79) Ong, S. P.; Richards, W. D.; Jain, A.; Hautier, G.; Kocher, M.; Cholia, S.; Gunter, D.; Chevrier, V. L.; Persson, K. A.; Ceder, G. *Comput. Mater. Sci.* **2013**, *68*, 314−319.
(80) Ong, S. P.; Jain, A.; Hautier, G.; Kang, B.; Ceder, G. *Electrochem. Commun.* **2010**, *12*, 427−430.
(81) McQuarrie, D. A. *Statistical Mechanics*; University Science Books: Sausalito, CA, 2000.
(82) McQuarrie, D. A.; Simon, J. D. *Molecular Thermodynamics*; University Science Books: Sausalito, CA, 1999.
(83) Gross, A.; Scheffler, J. *J. Vac. Sci. Technol. A* **1997**, *15*, 1624.
(84) Chase, M. W. *J. Phys. Chem. Ref. Data* **1998**, No. Monograph 9, 1−1951.
(85) Kresse, G.; Hafner, J. *Phys. Rev. B* **1993**, *47*, 558−561.
(86) Kresse, G.; Hafner, J. *Phys. Rev. B* **1994**, *49*, 14251−14269.
(87) Kresse, G.; Furthmüller, J. *Phys. Rev. B* **1996**, *54*, 11169−11186.
(88) Kresse, G.; Furthmüller, J. *Comput. Mater. Sci.* **1996**, *6*, 15−50.
(89) Sholl, D. S.; Steckel, J. A. *Density Functional Theory: A Practical Introduction*; John Wiley & Sons: Hoboken, NJ, 2009.
(90) Blöchl, P. E. *Phys. Rev. B* **1994**, *50*, 17953−17979.
(91) Kresse, G.; Joubert, D. *Phys. Rev. B* **1999**, *59*, 1758−1775.
(92) Perdew, J. P.; Chevary, J. A.; Vosko, S. H.; Jackson, K. A.; Pederson, M. R.; Singh, D. J.; Fiolhais, C. *Phys. Rev. B* **1992**, *46*, 6671−6687.
(93) Kresse, G.; Marsman, M.; Furthmüller, J. *Vienna Ab-Initio Simulation Package: VASP the Guide*; Computational Materials Physics: Vienna, 2014.
(94) Jain, A.; Hautier, G.; Moore, C. J.; Ping Ong, S.; Fischer, C. C.; Mueller, T.; Persson, K. A.; Ceder, G. *Comput. Mater. Sci.* **2011**, *50*, 2295−2310.
(95) Curtarolo, S.; Setyawan, W.; Hart, G. L. W.; Jahnatek, M.; Chepulskii, R. V.; Taylor, R. H.; Wang, S.; Xue, J.; Yang, K.; Levy, O.; et al. *Comput. Mater. Sci.* **2012**, *58*, 218−226.
(96) Parlinski, K. *PHONON*; Computing for Materials: Krakow, 2005.
(97) Togo, A.; Oba, F.; Tanaka, I. *Phys. Rev. B* **2008**, *78*, No. 134106.
(98) Wolverton, C.; Ozoliņš, V.; Asta, M. *Phys. Rev. B* **2004**, *69*, No. 144109.
(99) Jain, A.; Ong, S. P.; Hautier, G.; Chen, W.; Richards, W. D.; Dacek, S.; Cholia, S.; Gunter, D.; Skinner, D.; Ceder, G.; et al. *APL Mater.* **2013**, *1*, No. 011002.
(100) Griessen, R.; Riesterer, T. *Top. Appl. Phys.* **1988**, *63*, 219−284.
(101) Veleckis, E. *J. Nucl. Mater.* **1979**, *79*, 20−27.
(102) Orecchini, F.; Naso, V., Analysis of the Main Energy Vectors. In *Energy Systems in the Era of Energy Vectors*; Springer: London, 2012; Vol. *8*, p 153.
(103) Physical Constants of Inorganic Compounds. In *CRC Handbook of Chemistry and Physics*, 88th ed.; CRC Press: Boca Raton, FL, 2007.
(104) Bortz, M.; Hewat, A.; Yvon, K. *J. Alloys Compd.* **1997**, *248*, L1−L4.
(105) Bortz, M.; Hewat, A.; Yvon, K. *J. Alloys Compd.* **1997**, *253*−*254*, 13−16.
(106) Sherman, S. R., Tritium, A. *Research and Collaboration Plan for the NGNP Project*; U.S. DOE, Savannah River National Laboratory: Aiken, SC, 2008.